Title: Intragenic DNA inversions expand bacterial coding capacity

Authors: Rachael B. Chanin[1]†, Patrick T. West[1]†, Ryan M. Park[1], Jakob Wirbel[1], Gabriella Z. M. Green[1], Arjun M. Miklos[1], Matthew O. Gill[2], Angela S. Hickey[2], Erin F. Brooks[1], Ami S. Bhatt[1,2]*

Affiliations:

† These authors contributed equally to this work, listed alphabetically by last name

[1]Department of Medicine (Hematology, Blood and Marrow Transplantation); Stanford, USA.

[2]Department of Genetics, Stanford University; Stanford, USA.

*Corresponding author. Email: asbhatt@stanford.edu

Abstract: Bacterial populations that originate from a single bacterium are not strictly clonal. Often, they contain subgroups with distinct phenotypes. Bacteria can generate heterogeneity through phase variation: a preprogrammed, reversible mechanism that alters gene expression levels across a population. One well studied type of phase variation involves enzyme-mediated inversion of specific intergenic regions of genomic DNA. Frequently, these DNA inversions flip the orientation of promoters, turning ON or OFF adjacent coding regions within otherwise isogenic populations. Through this mechanism, inversion can affect fitness, survival, or group dynamics. Here, we develop and apply bioinformatic approaches to discover thousands of previously undescribed phase-variable regions in prokaryotes using long-read datasets. We identify 'intragenic invertons', a surprising new class of invertible elements found entirely within genes, in bacteria and archaea. To date, inversions within single genes have not been described. Intragenic invertons allow a gene to encode two or more versions of a protein by flipping a DNA sequence within the coding region, thereby increasing coding capacity without increasing genome size. We experimentally characterize specific intragenic invertons in the gut commensal *Bacteroides thetaiotaomicron*, presenting a 'roadmap' for investigating this new gene-diversifying phenomenon.

One-Sentence Summary: Intragenic DNA inversions, identified using long-read sequencing datasets, are found in many phyla across the prokaryotic tree of life.

Introduction

Adaptation is a cornerstone of survival for any species. In the complex gut microenvironment, bacteria experience many stressors including nutritional and niche competition, oxidative and nitrosative stress, and antibiotics. To overcome these challenges, bacteria may activate specific response programs which alter transcriptional or translational profiles promoting survival during these conditions. Additionally, bacterial daughter cells may acquire mutations, such as single nucleotide variations or small insertions or deletions, within genes. These gene alterations can then promote survival in the right circumstances. For example, mutations in drug targets, efflux pumps, or their regulators can provide increased resistance to antibiotics [1,2]. While many of these gene-varying mutations in bacteria are semi-reproducible, meaning that nucleotide alterations will occur in the same region of a genome under a similar environmental stressor, most are not reversible and may be costly when the stimulus is removed [3].

Beyond mutations and small insertions and deletions, there are only a few known mechanisms for introducing gene variation in bacteria. These mechanisms include: alternative translational start sites or terminators, which enable the encoding of two or more different gene products from a single mRNA [4,5]; slipped-strand mispairing, which introduces replicative or translational changes that can alter bacterial gene sequence length [6]; and diversity generating retroelements [7], which can diversify a gene during reverse transcription and recombine in a novel gene variant. Outside of these rare gene-varying events, the typical prokaryotic 'one gene, one gene product' rule generally holds and is in stark contrast to nearly all Eukaryotes, in which a large proportion of transcribed genes can undergo alternative splicing to generate multiple protein isoforms from one gene.

One fairly prevalent mechanism of reversible adaptation in bacteria is phase variation. This is a preprogrammed and reversible mechanism that generates phenotypic diversity in a clonal population [8]. Phase variation can promote cooperativity by sharing resources between subgroups in a metabolically efficient way or through bet hedging by diversifying a population to protect from complete elimination in future selective events. One type of preprogrammed variation occurs through DNA inversion. Site-specific recombinases recognize a pair of inverted repeats in genomic DNA and invert the intervening DNA sequence [9]. In the first described

example, DNA inversion of a promoter sequence resulted in the switching of expression from one flagellar antigen (H1) to another (H2) in *Salmonella enterica* serovar Typhimurium. The change in antigen expression determined whether the bacterium was bound by antiserum, and thus was termed a 'phase-determining event'[10–12]. This DNA inversion, and the many others that have since been discovered, play critical adaptive roles in both commensal and pathogenic bacteria.

For decades, these invertible loci were identified individually. Then, computational approaches enabled higher-throughput discovery of these 'invertons' across the genomes of a small subset of specific bacterial species [13,14]. In 2019, Jiang *et al.* developed an elegant method that facilitated broad scale identification of 4,686 intergenic invertons (i.e., invertons between genes) through a search of 54,875 bacterial reference genomes [15], utilizing short-read mapping as evidence; however, short-reads cannot span entire invertons, which can range in lengths of up to multiple kbps [15]. The long length of many of these invertons causes short-read based inverton detection methods to be lower in sensitivity, as methods to detect invertons rely on reads that span one boundary of a given inverton. This means that only a small proportion of reads provide usable evidence for inverton detection. Similarly to Jiang *et al*., in early 2023, Milman *et al.* used a computational model to predict over 11,000 potential invertons that partially overlap with genes (partial intergenic) in >35,000 bacterial species. Partial intergenic invertons are sometimes referred to as shufflon systems; they function by flipping out homologous domains of enzymes, which can change their specificity [16,17]. Once Milman *et al.* predicted the candidate invertons, they then manually inspected publicly available long-read datasets, which led to the validation of 22 of the >11,000 predicted invertons [18]. Taken together, these two studies demonstrate that computational approaches can be a powerful method to identify invertible elements within many phyla. Furthermore, the ubiquity of both intergenic and shufflon-type invertons in bacterial genomes highlights their likely importance in affecting bacterial gene regulation and phenotypes.

While previous work has demonstrated the presence of intergenic and shufflon-type invertons, there are no reports to our knowledge of invertons that occur entirely within genes. Such invertons would represent a novel mechanism of preprogrammed gene variation in bacteria. Furthermore, with the advent of long-read sequencing technologies, and improvements in their accuracy, developing a long-read inverton finding workflow would be expected to improve sensitivity in inverton discovery and detection. Building off these concepts, here we find that the

same mechanisms that underlie intergenic and partially intergenic invertons can occur entirely within a gene. These intragenic invertons expand bacterial coding capacity by either recoding protein sequences within the inverted region or introducing premature stop codons. In both cases, intragenic invertons result in a single gene being able to produce two or more different protein products. We develop PhaVa, a long-read based tool to identify intragenic, intergenic, and partial intergenic invertons. By applying PhaVa to long read sequencing data for ~30,000 bacterial isolates from ~4,000 unique species, we find that intragenic invertons occur in many phyla across the prokaryotic tree of life. In particular, we focus on *Bacteroides thetaiotaomicron*, a model enteric commensal, and validate 10 intragenic invertons experimentally with particular focus on the inverton contained within the thiamine biosynthesis protein *thiC*. Finally, we make both the PhaVa software package and all of the identified invertons (intragenic, intergenic, and partial intergenic) publicly available.

Results

Most knowledge regarding bacterial genes and their regulation is based on bacteria that are studied in laboratory conditions. Because of this, invertons that provide a fitness advantage *in vivo* but may not be advantageous to fitness *in vitro* have likely been overlooked [19–21]. We therefore hypothesized that there are currently unknown gut-relevant invertons. To test our hypothesis, we endeavored to identify invertons in metagenomic sequencing data from longitudinally collected human stool samples from 149 adult and 21 pediatric patients undergoing hematopoietic cell transplantation [22,23] (Fig. 1A). These samples were selected given the varying and complex environments enteric bacteria would encounter over time, with many different stressors present such as chemotherapy, antibiotic treatment, variation in food intake, and inflammation. We hypothesized that these factors might induce inverton flipping.

In our efforts to comprehensively annotate invertons from this metagenomic data set, in which there are many different organisms represented in each sample, we first decided to examine invertons in organisms within the taxon Bacteroidetes. Bacteroidetes species are prevalent and typically highly abundant in the human gut, and many organisms within this taxon have known intergenic invertons [15]. To orthogonally confirm sequencing-based observations in subsequent microbiological and genetic experiments, we focused our analysis on *B.*

124 *thetaiotaomicron*, a genetically tractable species suitable for downstream experimental
125 manipulation. To identify invertons in *B. thetaiotaomicron*, we used PhaseFinder [15], a short-read,
126 reference-based inverton detection pipeline with *B. thetaiotaomicron* VPI-5482 (BTh) as the
127 reference genome, and with relaxed filters to increase sensitivity (see methods, Fig. 1A). As an
128 internal control to assess whether PhaseFinder could sensitively detect BTh invertons in our
129 metagenomic samples, we examined BTh's capsular polysaccharide (CPS) genes, a known set of
130 invertible loci. BTh has 8 loci that encode different CPS, 5 of which are controlled by invertible
131 promoters [24–26]. CPS are important mediators of phage susceptibility [27] and can modulate the host
132 immune system [28–30]. Using PhaseFinder on the patient sample datasets, we found read evidence
133 of all 5 CPS invertons in both the reference and inverted (flipped) orientations (fig. S1),
134 demonstrating that PhaseFinder is able to detect known invertons in these metagenomic samples
135 and that these samples have enough *Bacteroides* sequencing depth to identify invertons. Of note,
136 in the reference BTh genome, the invertible promoter for each of these 5 loci is in the 'OFF'
137 state by virtue of it being oriented in the opposite direction of the CPS genes. Similarly, *in vitro*
138 transcriptional analyses support the finding that the majority of invertible CPS loci are in the
139 OFF orientation [31], suggesting that in laboratory conditions, these loci are not transcriptionally
140 active. Finding read evidence of inversion for all invertible CPS loci suggests that the *in vivo*
141 patient datasets are an ideal environment to detect invertible events that are rare in laboratory-
142 grown bacteria but may be prevalent in bacteria living in more 'natural' ecological settings.
143 In addition to known intergenic invertons such as those in the CPS loci, we also found
144 read evidence of intragenic invertons in BTh across 132 short-read metagenomic samples (Fig.
145 1B). We use the term 'intragenic inverton' to describe invertible regions found entirely within
146 single genes. To date, the only description of invertible DNA sequences entirely within a gene
147 are in isolated cases of very short (7 bp) flips within mitochondrial DNA in certain pathogenic
148 states [32]. These 7 bp mitochondrial DNA flips are postulated to be the consequence of an
149 enzyme-independent event, and thus are different from what we predict here to be an invertase-
150 mediated, preprogrammed inversion. In the intragenic invertons that we observed, there were
151 two predicted consequences. In some cases, the intragenic inverton resulted in a portion of the
152 protein being "re-coded" (Fig. 1C). For example, we observed a 57 bp inversion in BT0375, the
153 invertase that is believed to flip the adjacent CPS1 invertible promoter. This intragenic inversion
154 changes the amino acid sequence of the 'flipped' region, and might alter the binding specificity

155 of the invertase, possibly changing the invertible repeats (IRs) that it targets for flipping or its
156 binding affinity for its cognate IRs. In other cases, the intragenic inverton resulted in the
157 introduction of a 'premature' stop codon, affecting the prediction of protein coding open reading
158 frames (ORFs). Often, inversion resulted in two predicted ORFs (called with Prodigal [33]). For
159 example, the inverton in the hybrid two-component system BT3786 occurs between two
160 predicted protein folding domains, and thus might untether the "sensing" and "response"
161 elements (Fig. 1D) of this signaling protein. However, we also observed intragenic inversions
162 that resulted in zero, one, three, or more ORFs. Taken together, we describe the discovery of
163 intragenic invertons and identify two types of invertons - those that are 'recoding' and those that
164 cause a 'premature stop'.

165 To validate these predicted intragenic invertons, we analyzed the DNA sequences in
166 these gene regions *in vitro*. We extracted DNA from wild-type BTh grown in either rich or
167 defined media and designed PCR primer sets that enabled us to amplify either the reference or
168 the inverted version (fig. S2). We tested 59 of the 63 predicted intragenic invertons and
169 confirmed that 10 of them had DNA molecules in both the reference and inverted orientation in
170 our laboratory-grown population of BTh (Fig. 1B, Table 1, Data S1). The 49 unconfirmed
171 intragenic invertons may be due to the absence of cues in the growth conditions required to flip
172 the locus to the inverted orientation and/or false positives from the metagenomic read-based
173 evidence.

174 As genomic structural variation often involves highly repetitive or low complexity
175 regions, short-reads are often not long enough to resolve these sequences [34], and thus short-read
176 based approaches would be predicted to have limited sensitivity. We, therefore, developed a
177 long-read based inverton predictor, PhaVa. PhaVa maps long-reads against both a forward
178 (identical to reference) and reverse orientation version of potential invertons (Fig. 2A). PhaVa's
179 accuracy is high because it requires long-reads that span the entire length of a given inverton in
180 order to make a 'call' about its orientation. To ensure accurate performance of PhaVa, we
181 optimized read mapping parameters by simulating long-read datasets from ten bacterial genomes
182 at various sequencing depths (Fig. 2B-C). The reads were generated from a reference genome,
183 and thus no invertons are expected and any detected would be false positives. In general, the
184 false positive rate was very low (mean false positive count per simulated sample of <0.1 in 9/10
185 species), with the exception of reads simulated from the *Bordetella pertussis* genome (Fig. 2D).

186 Further investigation revealed the false positives detected in *B. pertussis* were due to a single
187 putative inverton with inverted repeats longer than 750 bps, of which only a smaller portion of
188 the total length were detected by 'einverted', the computational tool used to detected inverted
189 repeats (fig. S3). In summary, our long-read based inverton predictor, PhaVa, demonstrates high
190 accuracy in resolving complex genomic structural variations, with only rare instances of false
191 positives observed.

192 To find invertons across prokaryotic genomes, we ran PhaVa on ~30,000 prokaryotic
193 isolate long-read datasets deposited on SRA. We limited our analysis to readsets belonging to
194 Bacteria or Archaea and with 50 Mbp or more of total sequencing, which resulted in our final
195 analysis containing results from ~4,000 unique species (fig. S4). The vast majority of these
196 datasets represented bacteria, with only 42 archaeal long-read sequencing datasets. In total, we
197 identified 4622 unique invertons, 3,468 of which are intergenic. Of note, compared to Jiang *et al.*
198 [15], we find invertons at a higher rate per sequencing dataset (0.15 vs 0.07) and per individual
199 isolate (1.15 v 0.09) highlighting the increased sensitivity of long-reads for detecting this type of
200 structural variation. Like Jiang *et al.* [15], we found that Bacteroidetes have a relatively large
201 number of intergenic invertons (673, Fig. 3A) and intergenic invertons per genome (2.26, Fig.
202 3B). Fusobacteria, Gammaproteobacteria, and Verrucomicrobia also have high numbers of
203 intergenic invertons per genome (Fig. 3B), with Verrucomicrobia having the highest number per
204 genome overall at 5.55 intergenic invertons per genome. In our dataset, Verrucomicrobia is
205 composed of only *Akkermansia* strains. As increases in *Akkermansia* abundance correlate with
206 protection against metabolic disease [35,36], there is interest in its use as a probiotic. However,
207 *Akkermansia* strains exhibit broad phenotypic diversity and differential gut colonization ability
208 [37], which may be attributable, in part, to the orientation of these varied intergenic invertons. In
209 addition to the intergenic invertons, we also identified 733 partial intergenic invertons (Fig. 3A).
210 Many of these partial intergenic invertons may form shufflon systems, and thus, as expected,
211 these invertons are significantly longer than intergenic or intragenic invertons (Fig. 3C, p=7.1e-
212 293 and p=7.6e-67 with a t-test, respectively). This finding of 733 partial intergenic invertons
213 adds to the 22 long-read-validated intergenic invertons recently reported by Milman *et al*. Thus,
214 our analysis of ~30,000 prokaryotic isolate long-read datasets from diverse species uncovered
215 both known and novel intergenic and partial intergenic invertons, shedding light on the

216 remarkable structural variability within prokaryotic genomes and emphasizing the heightened
217 sensitivity of long-read sequencing in this context.
218 Beyond intergenic and partial intergenic invertons, we also found evidence of intragenic
219 invertons across multiple phyla, including the major gut microbiome-related phyla,
220 Proteobacteria, Firmicutes and Bacteroidetes (Fig. 3A-B). We found the largest number of
221 intragenic invertons, 118, in Gammaproteobacteria, including from organisms such as
222 *Escherichia coli* and *Salmonella*; this is largely due to the abundance of samples for these
223 organisms in SRA and our dataset (~4,000 *E. coli* samples (fig. S4)), given that
224 Gammaproteobacteria have a relatively small number of intragenic invertons detected per
225 genome (0.09, Fig. 3B). Few long-read datasets for Archaea were available with 36 and 6 for
226 Euryarchaeota and Crenarchaeota, respectively. Despite this, 12 putative archaeal invertons were
227 identified; ten intergenic, one partial intergenic, and an intragenic inverton that introduces an
228 early stop in a adenylosuccinate synthase gene in *Salarchaeum sp. JOR-1* (42 total archaeal
229 genomes searched, Fig. 3A-B, Data S2). Chromosomal invertons have only been minimally
230 investigated in Archaea. However, our study and a recent computational analysis of phase
231 variable Type 1 restriction modification systems by Atack *et al.* [17] suggest that inverton-mediated
232 phase variation may be an important, yet understudied, regulatory mechanism in this domain.
233 The mean number of intragenic invertons per genome varied greatly between different phyla
234 (Fig. 3B) with Tenericutes, Betaproteobacteria, and Actinobacteria having a relatively high
235 number of intragenic invertons detected per genome, at 0.19, 0.32, and 0.21, respectively. The
236 distribution of inversion proportions of individual intragenic invertons was different from that of
237 intergenic invertons (Fig. 3D); intergenic inversions typically appeared to be in either an “ON" or
238 “OFF” state in a given sample - suggesting that all of the organisms within that population
239 shared the same biological ‘state’ of that inverton. By contrast, intragenic invertons more
240 commonly had inversion proportions somewhere between 0 and 1 (Fig. 3D), indicating presence
241 of both the forward and reverse orientations within a given ‘clonal’ sample. Invertons with a
242 100% or near 100% proportion in the ‘reverse’ orientation may also represent those that can no
243 longer be flipped, either due to mutations in the IR or loss of the invertase that flips the inverton.
244 Having cataloged these intragenic invertons, we next investigated whether specific gene
245 types or functions were enriched for the presence of intragenic invertons by doing a clade-
246 resolved enrichment analysis. We calculated gene set enrichments (using Pfam clan definitions

247 as gene sets) per genome, species, and genus, combining the genes from all genomes in a
248 specific clade (Fig. 3E, S5). We found six Pfam clans enriched across several genera with the
249 strongest and most consistent enrichments for the Pfam clans CL0123 (Helix-turn-Helix) and
250 CL0219 (RNase-H-like) (fig. S5). This indicates that intragenic invertons occur more frequently
251 than would be expected by chance in genes that have DNA binding or DNA/RNA modifying
252 activity.

253 As noted previously, we postulate that inverton orientation likely relates to the
254 environment of a bacterium, and that invertons are more likely to be in the non-reference
255 orientation in organisms that are living in their 'natural' ecological settings. Therefore, we also
256 ran PhaVa on 210 *de novo* assembled long-read metagenomes from the human gut [38,39], mapping
257 sequencing reads back to their respective metagenomic assemblies. This enabled us to detect
258 invertons that may be absent in isolated bacteria grown in laboratory cultures, but present *in vivo.*
259 Doing so, we identified over 3,500 putative invertons, largely from contigs assigned to the phyla
260 Bacteroidetes and Firmicutes (fig. S6A). In keeping with our model that invertons are more
261 likely to be 'active' *in vivo* than *in vitro*, significantly more invertons were identified per species
262 in the metagenomic samples than in the isolate sequencing samples (fig. S6B). We hypothesize
263 this is because bacteria grown as isolates in laboratory settings do not experience the wide range
264 of diverse environmental conditions that they do in their natural, polymicrobial habitats. Our
265 analysis of the metagenomic data with PhaVa suggests that bioinformatic analysis of isolate
266 genomes grown in laboratory conditions likely underestimates the number and range of invertons
267 that exist in microbes. Therefore, the invertons called from the isolate datasets can be thought of
268 as a 'minimal set', as isolate conditions may not be the ideal setting to uncover phase variable
269 regions relative to metagenomic samples or co-cultures.

270 Both short-read and long-read based analyses of metagenomic datasets revealed that
271 intragenic invertons exist. However, the biological consequences of inversion of these invertons
272 to the non-reference orientation is not known. Thus, to evaluate the phenotypic consequences of
273 a particularly prevalent inverton, we focused on an intragenic inverton that introduces a
274 premature-stop codon in the BTh BT0650 gene (thiamine biosynthesis protein ThiC) (Fig. 4).
275 Thiamine is an essential cofactor in many cellular biochemical processes and is essential for
276 nearly all organisms. Some organisms, such as humans and certain gut microbes, are fully reliant
277 on dietary, host, or other microbial sources for vitamins or their building blocks; others, like

278 many gut microbes, including BTh, have the capacity to biosynthesize thiamine, albeit at a large
279 energetic cost [40,41]. Thus, thiamine availability has been hypothesized to strongly influence
280 microbial community composition [42]. We chose to characterize the intragenic inverton in *thiC* as
281 this gene has a defined function in thiamine biosynthesis [43,44]. Specifically, the *thiC* gene
282 product, which encodes the enzyme 2-methyl-4-amino-5-hydroxymethylpyrimidine phosphate
283 (HMP-P) kinase, catalyzes the conversion of aminoimidazole ribotide (AIR) to 4-amino-5-
284 hydroxymethyl-2-methylpyrimidine (HMP) and forms a key wing in thiamine biosynthesis. In
285 addition to having a defined role, we detected intragenic inversion in both DNA and RNA in our
286 laboratory grown BTh strain (Fig. 4B).We predicted that the non-reference orientation of the
287 inverton introduces a premature stop codon in the *thiC* mRNA, which would result in a truncated
288 protein containing only the N-terminal "thiC associated domain" of the protein (Fig. 4A). The
289 exact function of this domain of the protein is not known, but it is required for enzyme function.
290 As noted previously, BTh can grow in the absence of exogenous thiamine as it can synthesize
291 thiamine *de novo,* however, strains that lack ThiC lose this ability. We hypothesized that
292 inversion of the invertible locus in *thiC* would interfere with thiamine biosynthesis, and would
293 phenocopy the ThiC null mutant.
294 To test the biological consequences of inversion, we generated 'locked' versions of the
295 *thiC* inverton that prevent inversion from occurring within the gene. Traditionally, locking
296 elements in a specific orientation is accomplished by mutating the nucleotides in the inverted
297 repeat regions required for inversion or by deleting the inverted sequences entirely.
298 Unfortunately, for intragenic invertons, deletion of these sequences or complete mutations would
299 alter the corresponding amino acid sequences and confound interpretation. We therefore
300 exploited the wobble position of the codon to maximize mismatches between the inverted
301 repeats. By mutating these residues, we introduced mismatches in 6 out of 11 positions of the
302 inverted repeat (fig. S7A). Using this method, we created a locked forward (reference
303 orientation) and a locked reverse (flipped intragenic inverton) *thiC* strain. We also generated a
304 *thiC* clean deletion strain.
305 Next, we grew wild-type BTh, locked forward, locked reverse, and the *thiC* knockout
306 strain in various concentrations of thiamine (Fig. 4C). The locked forward strain phenocopied the
307 wild-type strain, as it was able to grow to the same optical density regardless of whether
308 thiamine was added to the media. By contrast, the locked reverse strain mirrored the *thiC* knock-

309 out strain and was only able to grow to wild-type levels when 0.1 μM or greater thiamine was
310 added to the media. This finding confirms our expectation that the reverse version of the
311 intragenic inverton interferes with ThiC function.
312 Having found that the locked reverse strain of the *thiC* intragenic inverton phenocopies
313 the null mutant, we wondered whether there may be physiological circumstances that favor this
314 mutant over the wild-type or locked forward strain. A classical approach to assess the relative
315 fitness of two bacterial strains is to perform a competitive growth experiment. Thus, to test
316 whether the inverted form of the *thiC* inverton provides a fitness advantage in different
317 conditions, we competed the locked forward strain against the locked reverse strain in an equal
318 proportion in varying concentrations of thiamine. Each strain was chromosomally marked with a
319 different antibiotic resistance cassette. Then we determined the competitive index (CI), which is
320 the ratio of recovered locked forward bacteria to recovered locked reverse bacteria (Fig. 4D). To
321 account for any fitness advantages conferred by the antibiotic resistance cassettes, we repeated
322 the competition with the cassette swapped between the two strains. While results varied slightly
323 between these two complementary versions of the experiment, they were generally concordant.
324 Specifically, we found that as thiamine concentration increases in the media the advantage
325 conferred by the locked forward version of *thiC* was first diminished and then abolished at
326 concentrations above 0.01 μM. In one version, the locked reverse significantly outcompeted the
327 locked forward strain at 1 and 10 μM, whereas in the other the version the reverse significantly
328 outcompeted the locked forward at 0.01, 0.1, and 10 μM (fig. S7 B-C). Notably, at
329 physiologically relevant thiamine concentrations, in the human intestine 0.02-2uM [45], the locked
330 reverse strain was more fit than the locked forward strain. This finding complements previous
331 work showing that auxotrophs have a fitness advantage in conditions containing a low level of
332 exogenous metabolites when competing against prototrophic strains [46]. The reversible nature of
333 invertons would allow a subgroup to switch between phenotypes, whereas a simple loss of
334 function mutation would not. Taken together, we find evidence of a physiologically relevant
335 condition in which an intragenic inversion within the *thiC* gene may provide an energetic or
336 other form of competitive advantage, and thus might be adaptive.
337

338 **Discussion**

339

340 Bacterial genomes densely encode functional genetic programs as well as multiple layers
341 of bioregulation. These layers of programming can be accessed by varying transcription,
342 translation, or through genomic restructuring. One mechanism of genome restructuring and
343 resultant 'genomic plasticity' is through enzyme-mediated DNA inversions. Such inversions can
344 regulate transcription of specific genetic loci through the flipping of promoter orientation
345 [10,15,47,48]. Furthermore, DNA inversions can also regulate shufflon systems that recombine
346 modular domains of bacterial protein-encoding genes to alter enzyme specificity [18,49,50]. To date,
347 entirely within-gene DNA inversions have not been described in prokaryotes. While not present
348 in every genome, the identification of enzyme-mediated intragenic inversions is important as it
349 represents another mechanism of genetic variation, and a way in which a single genetic locus can
350 encode multiple genes.
351 Here, we used short-read metagenomic data and a database of publicly available isolate
352 long-read sequencing to identify intragenic invertons in prokaryotes. In addition to using an
353 existing short-read inverton calling program, we developed a long-read inverton finding pipeline,
354 PhaVa, to more sensitively enumerate invertons. We identified intragenic invertons across the
355 prokaryotic tree of life, in both bacteria and the small number of archaea that we evaluated.
356 Using BTh as a model organism, we experimentally validated 10 intragenic invertons identified
357 from our short-read metagenomic analysis. We further assessed the consequence of inversion by
358 characterizing the phenotypic effects of an intragenic inverton found in the BTh thiamine
359 biosynthesis gene *thiC*. Thiamine is an essential cofactor for many central metabolic processes
360 and is bio-energetically costly to produce. Many microbes encode salvage, transport, and
361 biosynthetic pathways [51]. In BTh, thiamine acquisition and biosynthesis is highly regulated at
362 both the transcriptional and translational level [43,52]. Here, we find that thiamine biosynthesis also
363 appears to be regulated at the genomic structural level. The *thiC* intragenic inverton induces a
364 premature stop codon and we found that the truncated 'reverse' isoform has impaired growth in
365 thiamine-limited conditions. However, we also found that at physiological concentrations of
366 thiamine found in the human intestinal lumen, organisms encoding a locked 'reverse' isoform of
367 *thiC* have a competitive growth advantage over the locked 'forward' isoform. This supports the
368 presence of a novel mechanism of thiamine biosynthesis regulation and suggests a possible
369 ecological explanation for the existence of a 'toggle-able' switch of isoforms.

370 While the advantages of each identified intragenic inverton will differ depending on the
371 coding region affected, there are three general biological consequences of phase variation. One
372 reason an organism may have preprogrammed heterogeneity is to enable division of labor. By
373 generating subgroups within a population, members of the community may produce public goods
374 at a potential cost to their own fitness but for the benefit of the group as a whole [53–56]. While
375 altruism in bacterial interspecies relationships is often unstable, as cheaters will take advantage
376 of the public goods and outcompete, intraspecies altruism could bypass this as the losers in this
377 scenario can be repopulated by the winners [57]. The second type of heterogeneity producing
378 behavior is via a bet hedging strategy [58]. Diverse subgroups are generated allowing for survival
379 in future selection events. One classic example of this is the CPS switching that occurs in many
380 gut bacteria. As different CPS have varying susceptibility to phage predation, a diversified
381 population allows the species to persist in the presence of phage [27]. Third, bacteria of a given
382 species and strain may exist in various biogeographic 'niches', where neighboring bacteria, host
383 cells, nutrient access, and stressors might vary - thus, within a given ecological system such as
384 the intestinal lumen, different subcommunities of bacteria may benefit from employing different
385 bioregulatory programs. Future mechanistic work is needed to determine the advantages and
386 community structure implications of each intragenic inverton.
387 Although we validated the presence of the intragenic invertons in BTh, we have not
388 identified which invertases are responsible for each of the validated intragenic invertons that we
389 described. We suspect that an underlying "molecular grammar" exists and that certain invertases
390 recognize and flip specific sequences; specificity of invertases for a given sequence likely lie in
391 the inverted repeats, but might also lie within the inverted regions. In terms of how the
392 expression of these invertases is controlled and regulated in bacteria, phenotypic diversity is
393 often generated via two different mechanisms; random [57] or coordinated specialization [59]. It is
394 possible that invertases function at a basal level and therefore there is a baseline, low level of
395 inversion that occurs in a small proportion of the population. Alternatively, invertases may be
396 expressed in response to specific cues or signals. As BTh encodes 56 invertases, future work is
397 needed to identify which invertase flips these invertons and under which conditions.
398 Understanding how these elements are regulated and the consequences of inversion could
399 advance the field of synthetic biology and create new therapeutic targets.

400 Intragenic invertons that cause recoding mutations present an exciting opportunity to
401 rethink gene variation. In BTh, we molecularly confirmed 2 recoding intragenic invertons (Table
402 1). Of note, these recoding mutations may help regulate the outer membrane of a bacterial cell
403 potentially altering interactions with the host or other microbes. The first is BT0375, the putative
404 CPS1 invertase. Cross regulation of CPS loci has been well described [60,61]. Changes to the
405 invertase structure could change its binding specificity and alter which regions it flips or its
406 kinetics. Future studies are needed to elucidate how this inversion may add another layer of
407 regulation to which CPS loci are expressed and when they are expressed. The second is *nagA*
408 which encodes an enzyme that catalyzes the deacetylation of N-acetylglucosamine-6-phosphate
409 (GlcNAc-6-P) to glucosamine-6-phosphate (GlcN-6-P). NagA is important for cell wall
410 recycling and can supply GlcN-6-P for glycolysis [62]. As NagA can be allosterically regulated [63],
411 intragenic inversion could alter the binding of its allosteric regulator, altering this process; this
412 might result in changing the metabolism of the cell or the outer membrane structure. Bacterial
413 outer membranes play crucial roles in microbial interactions, niche establishment, and immune
414 modulation. Intragenic invertons may add another layer of regulation and future studies are
415 needed to study their effects.
416 While we find fairly extensive evidence of intragenic invertons using sequencing based
417 approaches and explore some of them in detail, this work has limitations. First, our analysis of
418 invertons across the prokaryotic tree of life was performed on previously sequenced isolates.
419 While growth conditions for most of these samples are not readily available, we presume that
420 most of these isolates were grown in rich laboratory media; these nutrient- and micronutrient-
421 replete conditions may not recapitulate physiological conditions in which invertases are active or
422 reverse orientations are favorable. However, there are currently limited long-read datasets
423 available from physiological conditions for a wide range of prokaryotic organisms. We therefore
424 may have only identified a minimal set of invertons in this study and we estimate the full
425 "invertome" likely includes a larger number of elements. Second, if the invertons we identified
426 are not representative of the true capacity for inversion, our gene set enrichment analysis may
427 also not identify the types of genes hit most frequently in physiological conditions. Third, both
428 PhaVa and PhaseFinder are reliant upon a reference genome or *de novo* assembly for read
429 mapping and selection of a particular sequence for read mapping can affect inverton discovery.
430 Detection of invertons is thus restricted to the genomic sequence common between the input

sequenced strain and the reference. Finally, PhaVa uses relatively strict mapping parameters and if the selected reference is distantly related to the sequenced strain, read mapping quality will decrease and reduce the discovery rate. However, using a *de novo* assembly instead may result in missing 'fully inverted' invertons relative to reference strains, which may be of interest.

Despite these limitations, intragenic invertons are an exciting new mechanism for genetic variation and adaptation in bacteria. In this manuscript, we present a 'roadmap' for more in depth investigation of a specific invertible intragenic locus. Our initial analysis of long-read isolate data provides a minimal set of invertons, including intragenic, intergenic, and partial intergenic invertons. We expect future niche-specific investigation of inverton-containing organisms to identify additional invertons. Additionally, we anticipate that future studies of intragenic inverton will uncover new layers of bioregulation in prokaryotes, and more thoroughly demonstrate the many hidden genetic programs that exist within highly plastic bacterial genomes. More thorough characterization of invertons and other reversible and preprogrammed types of genomic variation will likely substantially impact several fields of research ranging from synthetic biology, to microbe-microbe interactions, to microbial physiology, and beyond.

References

1. Hooper, D. C. & Jacoby, G. A. Mechanisms of drug resistance: quinolone resistance. *Ann. N. Y. Acad. Sci.* **1354**, 12–31 (2015).
2. Woodford, N. & Ellington, M. J. The emergence of antibiotic resistance by mutation. *Clin. Microbiol. Infect.* **13**, 5–18 (2007).
3. Björkman, J. & Andersson, D. I. The cost of antibiotic resistance from a bacterial perspective. *Drug Resist. Updat.* **3**, 237–245 (2000).
4. Meydan, S., Vázquez-Laslop, N. & Mankin, A. S. Genes within Genes in Bacterial Genomes. *Microbiol Spectr* **6**, (2018).
5. Zhong, A. *et al.* Toxic antiphage defense proteins inhibited by intragenic antitoxin proteins. *Proc. Natl. Acad. Sci. U. S. A.* **120**, e2307382120 (2023).
6. Moxon, R., Bayliss, C. & Hood, D. Bacterial contingency loci: the role of simple sequence

461 DNA repeats in bacterial adaptation. *Annu. Rev. Genet.* **40**, 307–333 (2006).
462 7. Medhekar, B. & Miller, J. F. Diversity-generating retroelements. *Curr. Opin. Microbiol.* **10**,
463 388–395 (2007).
464 8. van der Woude, M. W. & Bäumler, A. J. Phase and antigenic variation in bacteria. *Clin.*
465 *Microbiol. Rev.* **17**, 581–611, table of contents (2004).
466 9. Trzilova, D. & Tamayo, R. Site-Specific Recombination - How Simple DNA Inversions
467 Produce Complex Phenotypic Heterogeneity in Bacterial Populations. *Trends Genet.* **37**,
468 59–72 (2021).
469 10. Zieg, J., Silverman, M., Hilmen, M. & Simon, M. Recombinational switch for gene
470 expression. *Science* **196**, 170–172 (1977).
471 11. Andrewes, F. W. Studies in group-agglutination I. The salmonella group and its antigenic
472 structure. *J. Pathol. Bacteriol.* **25**, 505–521 (1922).
473 12. Stocker, B. A. Measurements of rate of mutation of flagellar antigenic phase in Salmonella
474 typhi-murium. *J. Hyg.* **47**, 398–413 (1949).
475 13. Goldberg, A., Fridman, O., Ronin, I. & Balaban, N. Q. Systematic identification and
476 quantification of phase variation in commensal and pathogenic Escherichia coli. *Genome*
477 *Med.* **6**, 112 (2014).
478 14. Sekulovic, O. *et al.* Genome-wide detection of conservative site-specific recombination in
479 bacteria. *PLoS Genet.* **14**, e1007332 (2018).
480 15. Jiang, X. *et al.* Invertible promoters mediate bacterial phase variation, antibiotic resistance,
481 and host adaptation in the gut. *Science* **363**, 181–187 (2019).
482 16. Komano, T. Shufflons: multiple inversion systems and integrons. *Annu. Rev. Genet.* **33**,
483 171–191 (1999).
484 17. Atack, J. M., Guo, C., Yang, L., Zhou, Y. & Jennings, M. P. DNA sequence repeats identify
485 numerous Type I restriction-modification systems that are potential epigenetic regulators
486 controlling phase-variable regulons; phasevarions. *FASEB J.* **34**, 1038–1051 (2020).
487 18. Milman, O., Yelin, I. & Kishony, R. Systematic identification of gene-altering programmed
488 inversions across the bacterial domain. *Nucleic Acids Res.* **51**, 553–573 (2023).
489 19. Chatzidaki-Livanis, M., Coyne, M. J., Roche-Hakansson, H. & Comstock, L. E. Expression
490 of a uniquely regulated extracellular polysaccharide confers a large-capsule phenotype to
491 Bacteroides fragilis. *J. Bacteriol.* **190**, 1020–1026 (2008).

492 20. Taketani, M., Donia, M. S., Jacobson, A. N., Lambris, J. D. & Fischbach, M. A. A Phase-
493 Variable Surface Layer from the Gut Symbiont Bacteroides thetaiotaomicron. *MBio* **6**,
494 e01339–15 (2015).
495 21. Troy, E. B., Carey, V. J., Kasper, D. L. & Comstock, L. E. Orientations of the Bacteroides
496 fragilis capsular polysaccharide biosynthesis locus promoters during symbiosis and
497 infection. *J. Bacteriol.* **192**, 5832–5836 (2010).
498 22. Severyn, C. J. *et al.* Microbiota dynamics in a randomized trial of gut decontamination
499 during allogeneic hematopoietic cell transplantation. *JCI Insight* **7**, (2022).
500 23. Siranosian, B. A. *et al.* Rare transmission of commensal and pathogenic bacteria in the gut
501 microbiome of hospitalized adults. *Nat. Commun.* **13**, 586 (2022).
502 24. Martens, E. C., Chiang, H. C. & Gordon, J. I. Mucosal glycan foraging enhances fitness and
503 transmission of a saccharolytic human gut bacterial symbiont. *Cell Host Microbe* **4**, 447–
504 457 (2008).
505 25. Martens, E. C., Roth, R., Heuser, J. E. & Gordon, J. I. Coordinate regulation of glycan
506 degradation and polysaccharide capsule biosynthesis by a prominent human gut symbiont.
507 *J. Biol. Chem.* **284**, 18445–18457 (2009).
508 26. Krinos, C. M. *et al.* Extensive surface diversity of a commensal microorganism by multiple
509 DNA inversions. *Nature* **414**, 555–558 (2001).
510 27. Porter, N. T. *et al.* Phase-variable capsular polysaccharides and lipoproteins modify
511 bacteriophage susceptibility in Bacteroides thetaiotaomicron. *Nat Microbiol* **5**, 1170–1181
512 (2020).
513 28. Round, J. L. *et al.* The Toll-like receptor 2 pathway establishes colonization by a
514 commensal of the human microbiota. *Science* **332**, 974–977 (2011).
515 29. Neff, C. P. *et al.* Diverse Intestinal Bacteria Contain Putative Zwitterionic Capsular
516 Polysaccharides with Anti-inflammatory Properties. *Cell Host Microbe* **20**, 535–547 (2016).
517 30. Mazmanian, S. K., Liu, C. H., Tzianabos, A. O. & Kasper, D. L. An immunomodulatory
518 molecule of symbiotic bacteria directs maturation of the host immune system. *Cell* **122**,
519 107–118 (2005).
520 31. Porter, N. T., Canales, P., Peterson, D. A. & Martens, E. C. A Subset of Polysaccharide
521 Capsules in the Human Symbiont Bacteroides thetaiotaomicron Promote Increased
522 Competitive Fitness in the Mouse Gut. *Cell Host Microbe* **22**, 494–506.e8 (2017).

523 32. Musumeci, O. *et al.* Intragenic inversion of mtDNA: a new type of pathogenic mutation in a
524 patient with mitochondrial myopathy. *Am. J. Hum. Genet.* **66**, 1900–1904 (2000).
525 33. Hyatt, D. *et al.* Prodigal: prokaryotic gene recognition and translation initiation site
526 identification. *BMC Bioinformatics* **11**, 119 (2010).
527 34. West, P. T., Chanin, R. B. & Bhatt, A. S. From genome structure to function: insights into
528 structural variation in microbiology. *Curr. Opin. Microbiol.* **69**, 102192 (2022).
529 35. Dao, M. C. *et al.* Akkermansia muciniphila and improved metabolic health during a dietary
530 intervention in obesity: relationship with gut microbiome richness and ecology. *Gut* **65**,
531 426–436 (2016).
532 36. Greninger, A. L. *et al.* Clinical metagenomic identification of Balamuthia mandrillaris
533 encephalitis and assembly of the draft genome: the continuing case for reference genome
534 sequencing. *Genome Med.* **7**, 113 (2015).
535 37. Becken, B. *et al.* Genotypic and Phenotypic Diversity among Human Isolates of
536 Akkermansia muciniphila. *MBio* **12**, (2021).
537 38. Chen, L. *et al.* Short- and long-read metagenomics expand individualized structural
538 variations in gut microbiomes. *Nat. Commun.* **13**, 3175 (2022).
539 39. Maghini, D. *et al.* Achieving quantitative and accurate measurement of the human gut
540 microbiome. *bioRxiv* 2022.09.28.509972 (2022) doi:10.1101/2022.09.28.509972.
541 40. Rodionov, D. A. *et al.* Micronutrient Requirements and Sharing Capabilities of the Human
542 Gut Microbiome. *Front. Microbiol.* **10**, 1316 (2019).
543 41. Sharma, V. *et al.* B-Vitamin Sharing Promotes Stability of Gut Microbial Communities.
544 *Front. Microbiol.* **10**, 1485 (2019).
545 42. Yatsunenko, T. *et al.* Human gut microbiome viewed across age and geography. *Nature*
546 **486**, 222–227 (2012).
547 43. Costliow, Z. A. & Degnan, P. H. Thiamine Acquisition Strategies Impact Metabolism and
548 Competition in the Gut Microbe Bacteroides thetaiotaomicron. *mSystems* **2**, (2017).
549 44. Martinez-Gomez, N. C. & Downs, D. M. ThiC is an [Fe-S] cluster protein that requires
550 AdoMet to generate the 4-amino-5-hydroxymethyl-2-methylpyrimidine moiety in thiamin
551 synthesis. *Biochemistry* **47**, 9054–9056 (2008).
552 45. Said, H. M. Intestinal absorption of water-soluble vitamins in health and disease. *Biochem.*
553 *J* **437**, 357–372 (2011).

554 46. D'Souza, G. *et al.* Less is more: selective advantages can explain the prevalent loss of
555 biosynthetic genes in bacteria. *Evolution* **68**, 2559–2570 (2014).
556 47. Abraham, J. M., Freitag, C. S., Clements, J. R. & Eisenstein, B. I. An invertible element of
557 DNA controls phase variation of type 1 fimbriae of Escherichia coli. *Proc. Natl. Acad. Sci.*
558 *U. S. A.* **82**, 5724–5727 (1985).
559 48. Weinacht, K. G. *et al.* Tyrosine site-specific recombinases mediate DNA inversions
560 affecting the expression of outer surface proteins of Bacteroides fragilis. *Mol. Microbiol.*
561 **53**, 1319–1330 (2004).
562 49. Nakayama-Imaohji, H. *et al.* Identification of the site-specific DNA invertase responsible
563 for the phase variation of SusC/SusD family outer membrane proteins in Bacteroides
564 fragilis. *J. Bacteriol.* **191**, 6003–6011 (2009).
565 50. Li, J.-W., Li, J., Wang, J., Li, C. & Zhang, J.-R. Molecular Mechanisms of hsdS Inversions
566 in the cod Locus of Streptococcus pneumoniae. *J. Bacteriol.* **201**, (2019).
567 51. Jurgenson, C. T., Ealick, S. E. & Begley, T. P. Biosynthesis of Thiamin Pyrophosphate.
568 *EcoSal Plus* **3**, (2009).
569 52. Rodionov, D. A., Vitreschak, A. G., Mironov, A. A. & Gelfand, M. S. Comparative
570 genomics of thiamin biosynthesis in procaryotes. New genes and regulatory mechanisms. *J.*
571 *Biol. Chem.* **277**, 48949–48959 (2002).
572 53. Veening, J.-W. *et al.* Transient heterogeneity in extracellular protease production by
573 Bacillus subtilis. *Mol. Syst. Biol.* **4**, 184 (2008).
574 54. Colizzi, E. S., van Dijk, B., Merks, R. M. H., Rozen, D. E. & Vroomans, R. M. A.
575 Evolution of genome fragility enables microbial division of labor. *Mol. Syst. Biol.* **19**,
576 e11353 (2023).
577 55. Chai, Y., Chu, F., Kolter, R. & Losick, R. Bistability and biofilm formation in Bacillus
578 subtilis. *Mol. Microbiol.* **67**, 254–263 (2008).
579 56. Marlow, V. L. *et al.* The prevalence and origin of exoprotease-producing cells in the
580 Bacillus subtilis biofilm. *Microbiology* **160**, 56–66 (2014).
581 57. Ackermann, M. *et al.* Self-destructive cooperation mediated by phenotypic noise. *Nature*
582 **454**, 987–990 (2008).
583 58. Grimbergen, A. J., Siebring, J., Solopova, A. & Kuipers, O. P. Microbial bet-hedging: the
584 power of being different. *Curr. Opin. Microbiol.* **25**, 67–72 (2015).

585 59. Kalamara, M., Spacapan, M., Mandic-Mulec, I. & Stanley-Wall, N. R. Social behaviours by
586 Bacillus subtilis: quorum sensing, kin discrimination and beyond. *Mol. Microbiol.* **110**,
587 863–878 (2018).
588 60. Chatzidaki-Livanis, M., Weinacht, K. G. & Comstock, L. E. Trans locus inhibitors limit
589 concomitant polysaccharide synthesis in the human gut symbiont Bacteroides fragilis. *Proc.*
590 *Natl. Acad. Sci. U. S. A.* **107**, 11976–11980 (2010).
591 61. Chatzidaki-Livanis, M., Coyne, M. J. & Comstock, L. E. A family of transcriptional
592 antitermination factors necessary for synthesis of the capsular polysaccharides of
593 Bacteroides fragilis. *J. Bacteriol.* **191**, 7288–7295 (2009).
594 62. Park, J. T. & Uehara, T. How bacteria consume their own exoskeletons (turnover and
595 recycling of cell wall peptidoglycan). *Microbiol. Mol. Biol. Rev.* **72**, 211–27, table of
596 contents (2008).
597 63. White, R. J. & Pasternak, C. A. The purification and properties of N-acetylglucosamine 6-
598 phosphate deacetylase from Escherichia coli. *Biochem. J* **105**, 121–125 (1967).
599 64. Bacic, M. K. & Smith, C. J. Laboratory maintenance and cultivation of bacteroides species.
600 *Curr. Protoc. Microbiol.* **Chapter 13**, Unit 13C.1 (2008).
601 65. Zhu, W. *et al.* Xenosiderophore Utilization Promotes Bacteroides thetaiotaomicron
602 Resilience during Colitis. *Cell Host Microbe* **27**, 376–388.e8 (2020).
603 66. Rice, P., Longden, I. & Bleasby, A. EMBOSS: the European Molecular Biology Open
604 Software Suite. *Trends Genet.* **16**, 276–277 (2000).
605 67. Li, H. Minimap2: pairwise alignment for nucleotide sequences. *Bioinformatics* **34**, 3094–
606 3100 (2018).
607 68. Yang, C., Chu, J., Warren, R. L. & Birol, I. NanoSim: nanopore sequence read simulator
608 based on statistical characterization. *Gigascience* **6**, 1–6 (2017).
609 69. De Coster, W., D'Hert, S., Schultz, D. T., Cruts, M. & Van Broeckhoven, C. NanoPack:
610 visualizing and processing long-read sequencing data. *Bioinformatics* **34**, 2666–2669
611 (2018).
612 70. Jumper, J. *et al.* Highly accurate protein structure prediction with AlphaFold. *Nature* **596**,
613 583–589 (2021).
614 71. Aramaki, T. *et al.* KofamKOALA: KEGG Ortholog assignment based on profile HMM and
615 adaptive score threshold. *Bioinformatics* **36**, 2251–2252 (2020).

616 72. Eddy, S. R. Accelerated Profile HMM Searches. *PLoS Comput. Biol.* **7**, e1002195 (2011).
617 73. Paysan-Lafosse, T. *et al.* InterPro in 2022. *Nucleic Acids Res.* **51**, D418–D427 (2023).
618 74. Benjamini, Y. & Hochberg, Y. Controlling the false discovery rate: A practical and
619 powerful approach to multiple testing. *J. R. Stat. Soc.* **57**, 289–300 (1995).
620 75. Prjibelski, A., Antipov, D., Meleshko, D., Lapidus, A. & Korobeynikov, A. Using SPAdes
621 De Novo Assembler. *Curr. Protoc. Bioinformatics* **70**, e102 (2020).
622 76. Lin, Y. *et al.* Assembly of long error-prone reads using de Bruijn graphs. *Proc. Natl. Acad.*
623 *Sci. U. S. A.* **113**, E8396–E8405 (2016).
624 77. Wood, D. E., Lu, J. & Langmead, B. Improved metagenomic analysis with Kraken 2.
625 *Genome Biol.* **20**, 257 (2019).
626 78. Li, W. & Godzik, A. Cd-hit: a fast program for clustering and comparing large sets of
627 protein or nucleotide sequences. *Bioinformatics* **22**, 1658–1659 (2006).
628 79. Koropatkin, N. M., Martens, E. C., Gordon, J. I. & Smith, T. J. Starch catabolism by a
629 prominent human gut symbiont is directed by the recognition of amylose helices. *Structure*
630 **16**, 1105–1115 (2008).
631 80. Simon, R., Priefer, U. & Pühler, A. A Broad Host Range Mobilization System for In Vivo
632 Genetic Engineering: Transposon Mutagenesis in Gram Negative Bacteria. *Biotechnology*
633 **1**, 784–791 (1983).
634 81. Pal, D., Venkova-Canova, T., Srivastava, P. & Chattoraj, D. K. Multipartite regulation of
635 rctB, the replication initiator gene of Vibrio cholerae chromosome II. *J. Bacteriol.* **187**,
636 7167–7175 (2005).

637

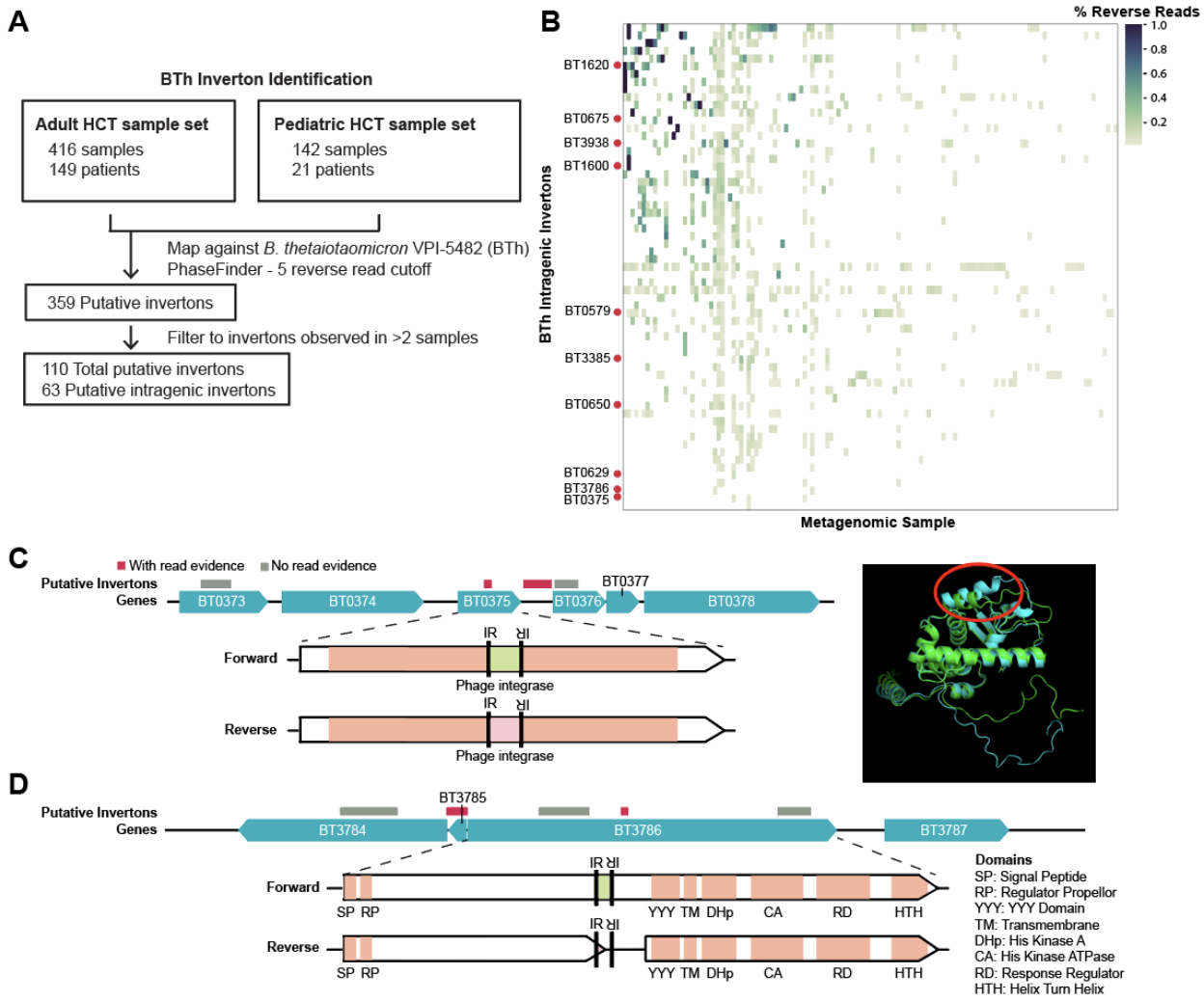

Fig. 1. Short-read metagenomic datasets reveal intragenic invertons in *Bacteroides thetaiotaomicron* (BTh). (**A**) An overview of the analysis pipeline for identifying putative invertons in short-read datasets. (**B**) A heatmap of the inversion proportion of intragenic invertons in BTh. Samples with no intragenic invertons were removed. Rows labeled with a gene name represent intragenic invertons with PCR and Sanger sequencing evidence of inversion. (**C-D**) Genome diagrams for confirmed intragenic invertons in BTh. Gray bars indicate putative invertons without sequencing support. Red bars indicate invertons with sequencing evidence. (**C**) Left - Genome diagram of the region surrounding the BT0375 recoding intragenic inverton, and a domain diagram of the BT0375 gene with the location of the inverton IRs indicated. Right - AlphaFold overlay of the BT0375 forward (blue) pLDDT 89.91 and reverse (green) pLDDT 85.24. The region that is recoded is circled in red. (**D**) Genome diagram of the region surrounding the BT3786 premature stop codon intragenic inverton, and a domain diagram of the gene. The consequence of the inversion and resulting two predicted ORFs are indicated in the domain diagram.

654
655
656

Gene	Annotation	Consequence
BT0375	integrase	recoding
BT0579	putative transcription regulator	premature stop codon
BT0629	Mn2+ and Fe2+ transport protein	premature stop codon
BT0650	thiamine biosynthesis protein ThiC	premature stop codon
BT0675	N-acetylglucosamine-6-phosphate deacetylase NagA	recoding
BT1600	BexA, membrane protein	premature stop codon
BT1620	SusD homolog	premature stop codon
BT3385	putative helicase	premature stop codon
BT3786	two-component system sensor histidine kinase/response regulator, hybrid (one-component system)	premature stop codon
BT3938	ATP-dependent DNA helicase RecQ	premature stop codon

657
658 **Table 1. Confirmed intragenic invertons BTh.** Intragenic invertons confirmed *in vitro* in BTh
659 are listed. Invertons from short-read datasets were called with PhaseFinder on metagenomic
660 samples (see Fig.1). The predicted consequence of inversion is also listed.

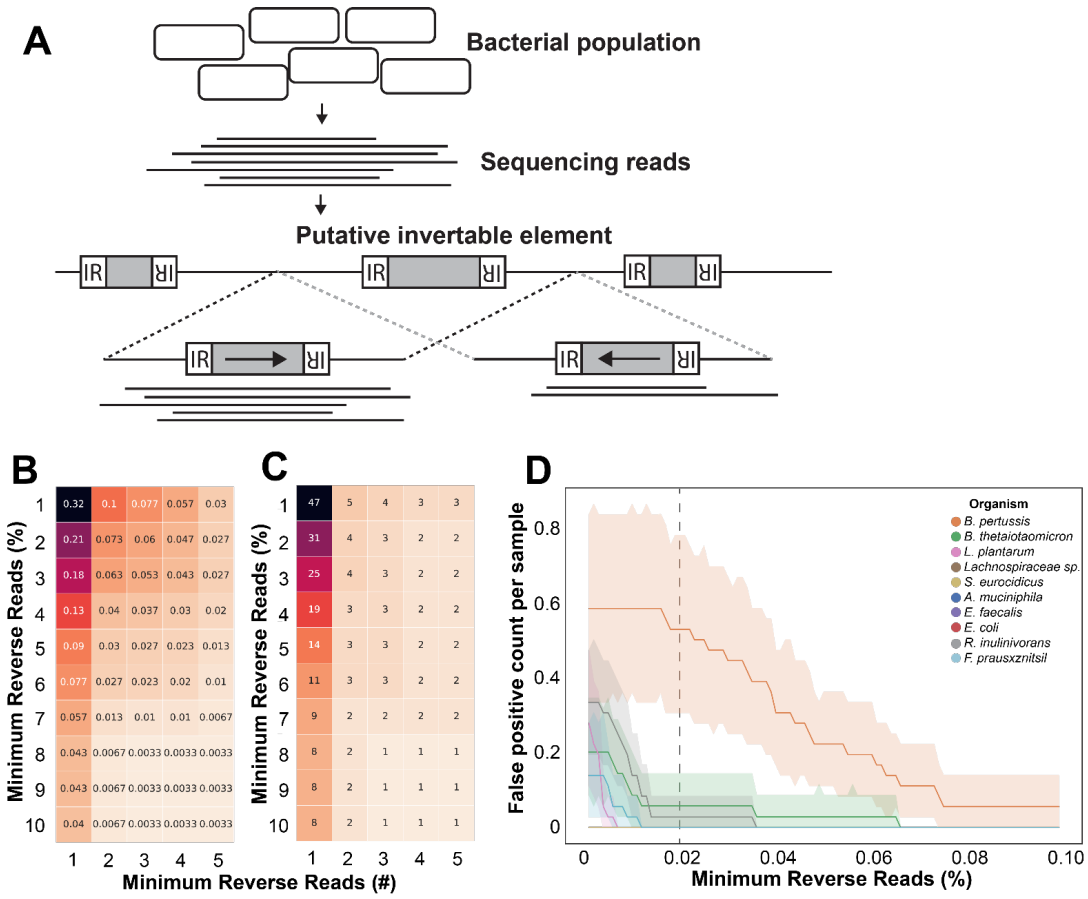

Fig. 2. Developing and optimizing PhaVa, a long-read based, accurate inverton caller. (A) Schematic of PhaVa's workflow. Putative invertons are identified, and long-reads are mapped to both a forward (highlighted by the black dashed lines) and reverse orientation (highlighted by the gray dashed lines) version of the inverton and surrounding genomic sequence, similar to PhaseFinder. Reads that do not map across the entire inverton and into the flanking sequence on either side, or have poor mapping characteristics are removed. See methods for details. **(B-C)** Optimizing cutoffs for the minimum number of reverse reads as both a raw number and percentage of all reads, to reduce false positive inverton calls with simulated reads. Cell color and number represent **(B)** the false positive rate per simulated readset and **(C)** the total number of unique false positives across all simulated datasets. **(D)** False positives in simulated data plotted per species. All measurements were made with a minimum of three reverse reads cutoff and varying the percentage of minimum reverse reads cutoff. Dashed line indicates the minimum reverse reads percent cutoff used for isolate and metagenomic datasets.

675

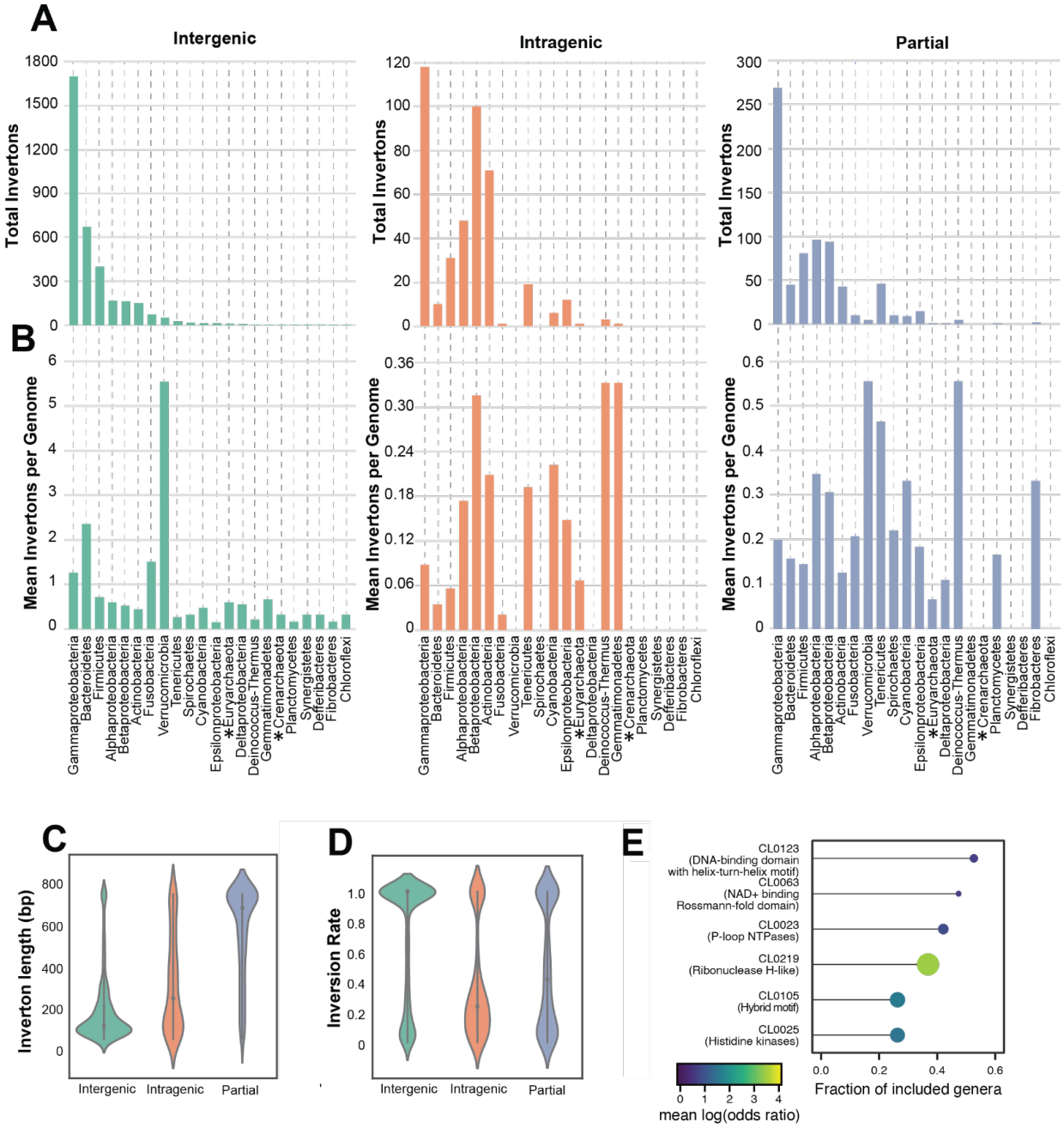
A
Intergenic
Intragenic
Partial
Total Invertons
B
Mean Invertons per Genome
Gammaproteobacteria
Bacteroidetes
Firmicutes
Alphaproteobacteria
Betaproteobacteria
Actinobacteria
Fusobacteria
Verrucomicrobia
Tenericutes
Spirochaetes
Cyanobacteria
Epsilonproteobacteria
*Euryarchaeota
Deltaproteobacteria
Deinococcus-Thermus
Gemmatimonadetes
*Crenarchaeota
Planctomycetes
Synergistetes
Defferibacteres
Fibrobacteres
Chloroflexi
C
Inverton length (bp)
Intergenic
Intragenic
Partial
D
Inversion Rate
E
CL0123
(DNA-binding domain
with helix-turn-helix motif)
CL0063
(NAD+ binding
Rossmann-fold domain)
CL0023
(P-loop NTPases)
CL0219
(Ribonuclease H-like)
CL0105
(Hybrid motif)
CL0025
(Histidine kinases)
Fraction of included genera
mean log(odds ratio)

676

677 **Fig. 3. PhaVa analysis of isolate long-read sequencing data reveals intragenic inversions are**
678 **prevalent across the bacterial tree of life**. (**A**) The total number of invertons found within
679 various bacterial phyla from 29,989 publicly available long-read isolate sequencing datasets.
680 Green bars refer to intergenic invertons. Orange bars refer to intragenic invertons. Blue bars refer
681 to partial intergenic invertons. Asterisks denote phyla within Archaea. Inset corresponds to the
682 portion of the bar graph outlined in dotted lines. (**B**) The mean number of invertons found per
683 genome within a phylum, of genomes that had at least one inverton. Asterisks denote phyla
684 within Archaea. (**C**) The distribution of lengths of identified invertons, grouped by inverton type
685 (intergenic, partial intergenic - denoted 'partial', and intragenic). Median value is indicated by
686 gray dots. Partial length distribution was found to be significantly different from intergenic
687 (p=0.0) and intragenic (p=4.5e-146) with a t-test (**D**) The distribution of inversion rates of
688 identified invertons, defined as the percentage of reads mapped in the reverse orientation.
689 Median value is indicated by gray dots. (**E**) Pfam clan enrichment across several genera. Dot size
690 and fill color is proportional to the mean log-odds ratio, an effect size measure for the
691 enrichment, and the length of the line indicates the fraction of included genera in which an
692 enrichment score for the specific clan could be calculated.
693

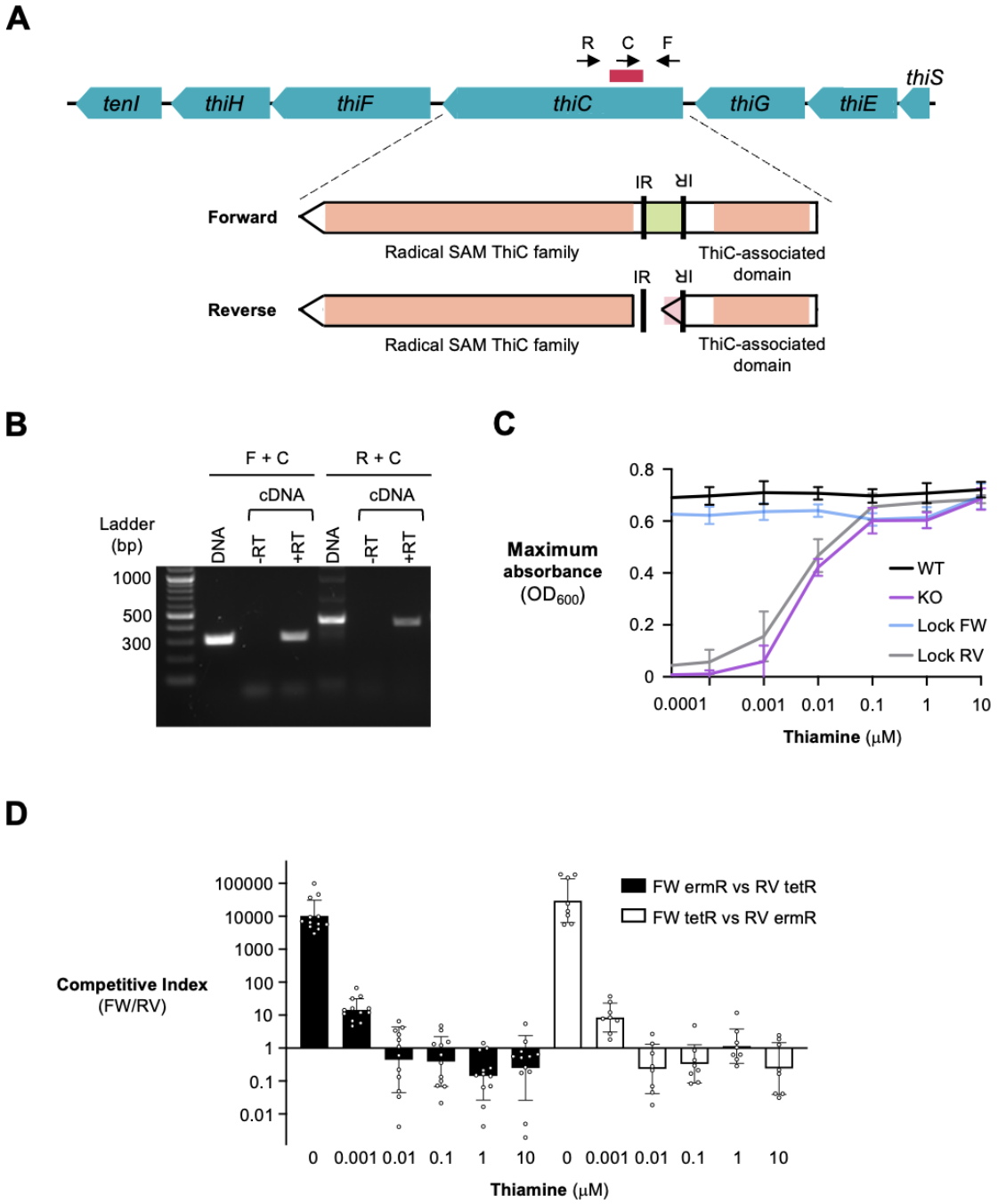

694

695 **Fig. 4. Consequences of inversion in thiamine biosynthesis protein (*thiC*).** (**A**) Schematic
696 showing the location of the *thiC* intragenic inverton (red bar). Inverton flipping results in a
697 premature stop codon located between two protein-folding domains in ThiC. Black arrows
698 indicate the binding location of primers used to determine the orientation of inverton. (**B**) PCR
699 confirmation of the *thiC* intragenic inverton in both genomic DNA and reverse transcribed RNA
700 (cDNA). PCR products of the expected size were extracted and confirmed with Sanger
701 sequencing. (**C**) BTh strains were grown in defined media with the indicated concentrations of
702 thiamine. The maximum optical density of each strain reached was recorded. Each point

703 represents the average of six replicates conducted across two separate experiments. Mean and
704 standard deviation are shown. Locked forward (blue line), locked reverse (gray line), *thiC*
705 knockout (purple line), and wild-type (black line) are presented. (**D**) Locked strains were
706 competed against each other in thiamine-containing media. The competitive growth experiment
707 was performed in two different ways with the antibiotic resistance marker cassettes flipped
708 between the two versions. Black bars indicate the locked forward strain marked with
709 erythromycin resistance and locked reverse strain marked with tetracycline resistance. White
710 bars indicate the locked forward strain marked with tetracycline resistance and locked reverse
711 strain marked with erythromycin resistance. The competitive index was determined. Geometric
712 mean and geometric standard deviation are shown for 8-12 replicates across 4-6 independent
713 experiments.
714

715 **Materials and Methods**

716

717 Strains and media

718

719 The bacterial strains used in this study are listed in Table S1. *E. coli* strains were routinely grown
720 in LB Miller media (Fisher) at 37 ℃. When necessary, carbenicillin was added at 100 µg/mL.
721 BTh was grown anaerobically (90% Nitrogen, 5% carbon dioxide, 5% hydrogen) in an anaerobic
722 chamber (Sheldon Manufacturing) in hemin (5 µg/mL) and L-cysteine (1 mg/mL) supplemented
723 Brain Heart Infusion (Sigma) media (BHIS) or Varel-Bryant broth (VB)[64]. When necessary, the
724 antibiotics tetracycline (2.5 µg/mL), erythromycin (25 µg/mL), or gentamicin (200 µg/mL) were
725 added to the media. Thiamine HCL (Sigma) was added at the specified concentrations. All media
726 used to grow BTh was preincubated in the anaerobic chamber overnight.

727

728 Construction of *thiC* clean deletion and locked strains

729

730 The *thiC* clean deletion and locked strains were generated via allelic exchange as previously
731 described [65]. For Δ*thiC*, 600 - 700 base pair flanking regions of the coding region were amplified
732 using Q5 high fidelity polymerase (New England Biolabs). Recombinant DNA used in this study
733 is listed in Table S2. For locked strains, plasmid overhangs, flanking regions, locked repeats and
734 intervening forward or inverted sequences were synthesized (Twist Biosciences) (Data S8).
735 Regions were assembled into pExchange-tdk using the HiFi DNA Assembly Kit (New England
736 Biolab). Plasmid inserts were verified using Sanger sequencing (ElimBio). Sequence confirmed
737 plasmids were propagated in *E. coli* DH5α λ*pir*. *E. coli* S17-1 λ*pir* was used as a donor strain for
738 conjugation into BTh Δ*tdk*. Exconjugants with chromosomal integration of plasmids were
739 recovered on BHIS plates containing gentamicin and erythromycin. Second crossover events
740 were selected by using BHIS FudR (200 µg/mL 5-fluoro-2-deoxy-uridine). Deletion and locked
741 versions were confirmed by PCR.

742

743 To generate differentially resistant *thiC* locked strains, the suicide vectors pNBU2_tet and
744 pNBU2_erm were used. *E. coli* S17-1 λ*pir* harboring the plasmids were used as donor strains for

745 conjugation. Single crossover events were selected by plating on gentamicin plates containing
746 either erythromycin or tetracycline respectively.

747 Validating inversion in DNA

748 Intragenic inverton confirmation primers were designed using NCBI Primer Blast under default
749 settings with the addition of adding in a GC clamp. PCR product size was targeted to be between
750 300 and 600 base pairs. The common and reverse primer were oriented on the same strand of the
751 reference genome and the forward primer was located on the complementary strand. The
752 common primer was located in between the two inverted repeats (fig. S2, primers listed in Data
753 S6). Four of the predicted invertons were not experimentally tested, as target-specific primers
754 could not be generated within the above constraints.

755 DNA was isolated from wild-type BTh cultures grown for 18 hours in either BHIS or VB media.
756 DNA was isolated using a chemical and enzymatic lysis. Glass beads (0.1 mm) were added to
757 bacterial pellets along with 700 µl of extraction buffer (50 mM Tris pH 7.5, 1 mM EDTA, 100
758 mM NaCl, 1% (w/v) SDS) and 25 µl of Proteinase K (10 mg/mL). Pellets were vortexed for 20
759 seconds and incubated at 55ºC for 60 min. 700 µl of phenol:chloroform:isoamyl alcohol (25:24:1
760 by volume) was added to the mixture prior to incubating at room temperature for 5 minutes.
761 Phases were separated by centrifuge at 10,000 rpm for 5 minutes. The aqueous upper layer was
762 collected and transferred to a new tube. 5 µl of RNAse A (10 mg/mL) was added and incubated
763 at 37ºC for 15 minutes. An equal volume of phenol:chloroform:isoamyl alcohol was added,
764 mixed, and incubated at room temperature for 5 minutes. Phases were separated as above and the
765 aqueous phase was added to a new tube containing an equal volume of chloroform: isoamyl
766 alcohol (24:1 by volume). Tubes were mixed and incubated at room temperature for 5 minutes
767 prior to phase separation via centrifugation. The aqueous phase was added to a new tube along
768 with 45 µl of 3M sodium acetate and 1 mL cold 100% ethanol. DNA was precipitated overnight
769 at -20ºC . Pellets were washed twice with 1mL of cold 70% ethanol. Dried pellets were
770 resuspended in water.

771 PCR reactions were performed using Q5 high fidelity polymerase (68 ℃ annealing temp, 10
772 second annealing time, and 30 second extension time). PCR reactions were run on an 1.2%
773 agarose gel. If multiple bands were visible, bands of the expected size were gel purified using the

774 Qiagen Gel Extraction kit. If a single band of the expected size was observed, the PCR reaction
775 was purified using the Monarch PCR Cleanup Kit (New England Biolabs). DNA was sent for
776 Sanger sequencing. Sequencing was compared to the *in silico* prediction.

777 Validating *thiC* inversion in RNA

778 RNA was isolated from wild-type BTh cultures grown for 18 hours in BHIS media. 5mL cultures
779 were quenched using 500 µL phenol/ethanol solution (90% [vol/vol] ethanol and 10% [vol/vol]
780 saturated phenol pH 4-5). Pellets were spun down and stored at -80 ℃ until extraction. Pellets
781 were lysed in 250 µL PBS and 10 µL of lysozyme (10 mg/mL) at 37 ℃ for 30 minutes. 30 µl
782 20% SDS was added prior to an additional 30 minute incubation. 1.5 mL Trizol was added to the
783 mixture and incubated at room temperature for 10 minutes. Chloroform (0.5 mL) was added to
784 each sample and inverted vigorously for 15 seconds. The aqueous phase was taken from
785 centrifuged samples and an equal volume of 100% ethanol was added. RNA was purified using
786 the Zymo RNA clean kit. DNA was removed using Ambion Turbo DNAse. cDNA was made
787 using Taqman Reverse Transcription reagents (Invitrogen) according to the manual. A no reverse
788 transcriptase control was performed to ensure that all DNA was removed. PCR was performed to
789 determine orientation of inverton as above. Correctly sized bands were sent for Sanger
790 sequencing.

791 BTh growth in thiamine concentrations

792 BTh wild-type, *thiC* locked forward, *thiC* locked reverse, and *thiC* knockout strains were grown
793 overnight in BHIS media. Aliquots of each were then washed twice in preincubated PBS
794 containing cysteine (1 mg/mL). Strains were inoculated at an OD600 of 0.05 in VB media
795 containing the indicated concentration of Thiamine in a 96-well flat bottom plate. Readings were
796 taken in a Stratus plate reader (Cerillo) every ten minutes. Non-inoculated VB media from each
797 time point was used as a blank. The maximum OD600 value achieved per well was determined.

798 Competitive growth assay

799 Marked BT0650 locked strains were grown overnight in BHIS with appropriate antibiotics.
800 Strains were washed twice with preincubated PBS containing cysteine (1 mg/mL). A glass
801 dilution tube containing 3 mL of VB with indicated concentrations of thiamine was inoculated

802 with 1 x 10^3 CFU/mL of each strain. After 40 hrs of growth at 37 ℃ in the anaerobic chamber,
803 CFU/mL was determined by plating on selective agar. A competitive index was calculated by
804 dividing the recovered CFU/mL of the locked forward by the CFU/mL of the locked reverse
805 strain corrected by the inoculum.

806 Identifying invertons in BTh with PhaseFinder

807 Two short-read datasets were used for identifying invertons in BTh, 416 samples from 149 adult
808 HMT patients ([23], BioProject PRJNA707487) and 142 samples from 21 pediatric HMT patients
809 ([22], BioProject PRJNA787952). Each individual short-read dataset was analyzed with
810 PhaseFinder [15] with the VPI-5482 reference genome and default parameters to identify putative
811 invertons in BTh. Invertons were included in further analysis if they had at least 5 reads mapping
812 to the reverse orientation of the inverton, and had reads mapping to the reverse orientation in at
813 least three different samples. Inverton-gene overlaps and partial overlaps were found using a
814 custom script, now incorporated in PhaVa in the 'Create' step, and the gene annotations from the
815 VPI-5482 genbank file (.gbff).

816 The PhaVa algorithm

817 Inverted repeats are identified with einverted, part of the EMBOSS suite [66]. For each putative
818 inverton, two sequences are then created: one where the sequence between identified inverted
819 repeat pairs is inverted (reverse) and one where it is not (forward), along with flanking sequence
820 on either side, similar to PhaseFinder. Long-reads are mapped against the created sequence with
821 minimap2 [67] and must pass several filters to be included as evidence of inversion. 1) reads must
822 have a MAPQ score of ≥ 2 to eliminate multimapping reads. 2) Reads must span the entire length
823 of the inverton and at least 30 bps into the flanking sequence on either side. 3) The mismatch rate
824 along the length of a read must be below a maximum mismatch rate. The mismatch rate is
825 considered separately over the length of an inverton and over flanking sequence, to avoid reads
826 that map well to only one region or the other. An adjustable mismatch rate is used instead of a
827 flat mismatch cutoff to account for both the variable length of long-reads and the high
828 sequencing error rate of current long-read sequencing technologies relative to short-read
829 sequencing. After mapping, reads mapped to the inverted and non-inverted sequences are tallied
830 and optional post-mapping filters are applied. 1) A minimum number of total reads mapped to

831 the ‘reverse’ sequence and 2) a minimum proportion of total mapped reads mapped to the
832 ‘reverse’ sequence.

833 Simulating long-read datasets for optimizing PhaVa

834 For benchmarking, ten bacterial species were selected, in part based on the relevance in the
835 human microbiome. For each species, a reference genome and reference long-read dataset were
836 obtained from NCBI (File S3). Long-reads were mapped against their respective reference
837 genome with minimap2 and the mappings were used as input for the ‘characterization stage’ of
838 NanoSim [68] in genome mode. The resulting NanoSim models were used to generate simulated
839 long-read datasets in the ‘simulation stage’ in genome mode. Reads were generated from the
840 unmodified reference genome, and so no evidence of inversion for any inverton is expected, and
841 any invertons identified by PhaVa would be false positives. For each species, five coverage
842 levels and six replicates of each coverage level were generated (Data S7) totaling in 300
843 simulated long-read datasets. *Streptomyces eurocidicus* and *Enterococcus faecalis* simulated
844 readsets were generated at relatively deeper coverages due to poor read mapping characteristics
845 from the selected reference long-read datasets resulting in a smaller proportion of reads passing
846 PhaVa read mapping filters. Simulated readsets were then analyzed with PhaVa and used to
847 estimate false positive rates and optimize post-mapping filters.

848 Identifying putative invertons from public long-read sequencing data with PhaVa

849 Candidate isolate long-read sequencing datasets were identified on NCBI with the following
850 search criteria: “(Bacteria[Organism] OR Archaea[Organism]) AND ("pacbio smrt"[Platform]
851 OR "oxford nanopore"[Platform]) AND genomic[Source]”. Datasets were further filtered by
852 removing datasets with the “amplicon” flag, and removing datasets with less than 50 Mbp of
853 sequencing in total (Data S5). Individual read datasets were downloaded with fastq-dump, a part
854 of the sratoolkit (https://trace.ncbi.nlm.nih.gov/Traces/sra/sra.cgi?view=software). Nanostat [69]
855 was run on each remaining readset to measure dataset characteristics. For each unique taxid
856 represented in the resulting readsets, a reference genome and paired genbank file (.gbff) were
857 selected by identifying a genome with the highest level of completion for that species, and the
858 least number of contigs. In the case of reference genomes with equal quality based on these
859 parameters, the first identified was selected. Long-read datasets were then analyzed with PhaVa

860 with default parameters. Gene overlaps and partial gene overlaps were identified by comparing
861 coordinates of genbank file annotations with inverton coordinates, a function available for use in
862 PhaVa (fig. S8).

863 AlphaFold prediction

864 Structural predictions of the amino acid sequences for the forward and reverse orientations of the
865 intragenic inverton within BT0375 were generated using AlphaFold [70] v2.2.0. The required
866 databases were downloaded on March 3rd, 2022 and the max template date was set to 2020-05-
867 14. The top ranked structures were then visualized and aligned in PyMOL.

868 Gene set enrichment analysis

869 In order to assess which functional groups were enriched for genes harboring intragenic
870 invertons, we performed a clade-resolved gene set enrichment analysis. We first annotated genes
871 with KEGG KOs using the kofamKOALA tool [71] and with Pfam domains by running HMMER3
872 [72] with the Pfam domain database. KEGG pathways and modules were filtered for those that
873 were present in bacterial genomes and Pfam clan definitions were downloaded from the Interpro
874 website [73]. We then calculated enrichments per genome and additionally per species and per
875 genus, for those combining the genes from all genomes in a specific clade. At each level, we
876 filtered out groups with fewer than 5 intragenic invertons (fig. S5), resulting in 10 genomes, 12
877 species, and 19 genera being included for downstream analysis. Alternatively, we also considered
878 genes with both intragenic or partial intergenic invertons, resulting in 47 genomes, 52 species, and 54
879 genera being tested. In each group, we tested for each pathway if the genes annotated with this
880 pathway were enriched for those carrying invertons by using a one-sided Fisher test. Pathways,
881 the genes of which did not harbor any invertons in a specific group, were skipped for the
882 enrichment analysis for a given group. Multiple testing correction was performed with the
883 Benjamini-Hochberg procedure [74].

884 Identifying putative invertons from long-read metagenomes.

885 200 hybrid short-read and long-read human stool metagenomic datasets were accessed from
886 BioProject PRJNA820119 [38]. Each hybrid dataset was assembled using SPAdes [75] with the '-
887 meta' flag and long-reads provided with the '--nanopore' option. An additional ten nanopore

888 long-read human stool microbiome metagenomic datasets from BioProject PRJNA940499 [39]
889 were assembled with Flye [76]. Assembled contigs will be deposited at
890 https://doi.org/10.5281/zenodo.7662825 after publication. Gene annotations for assemblies were
891 obtained with Prodigal [33] using the '-meta' flag. Contig taxonomic classifications were obtained
892 with Kraken2 [77]. Each long-read dataset was then analyzed with PhaVa with default parameters,
893 using its respective de novo assembly as its reference assembly. Resulting inverton calls were
894 dereplicated by clustering the inverton with 1000 bp flanking sequence upstream and
895 downstream at 99% average nucleotide identity with CD-HIT [78].
896
897

898 **Supplemental Figures**

899

900

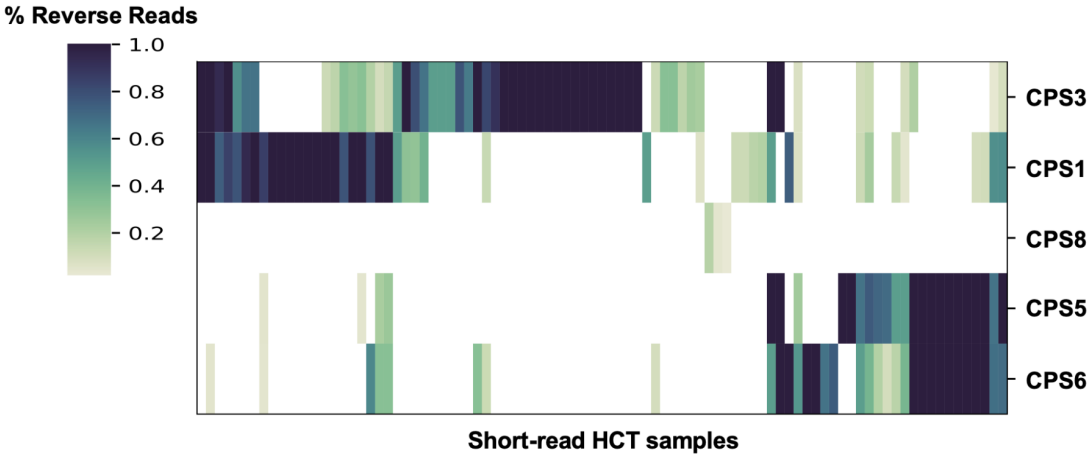

901

902 **Fig. S1. Inversion proportion of CPS loci invertons in BTh.** Inversion proportions of CPS loci
903 invertons in HCT metagenomic samples measured with PhaseFinder. Samples with no inversions
904 in the five CPS invertons were removed.

905

906

907

908

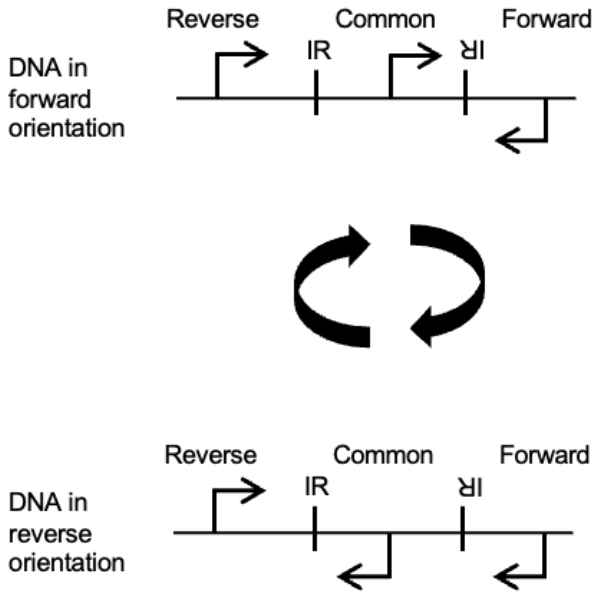

Fig. S2. Inverton confirmation PCR primer design. A Forward and Reverse primer bind to regions of the genome upstream and downstream of the inverton on opposite strands. The Common primer binds the DNA inside of the inverton, between the inverted repeats. When the DNA is in the forward orientation, the Common and Forward primer will generate a PCR product. When the inverton flips, the Common and Reverse primer will generate a PCR product.

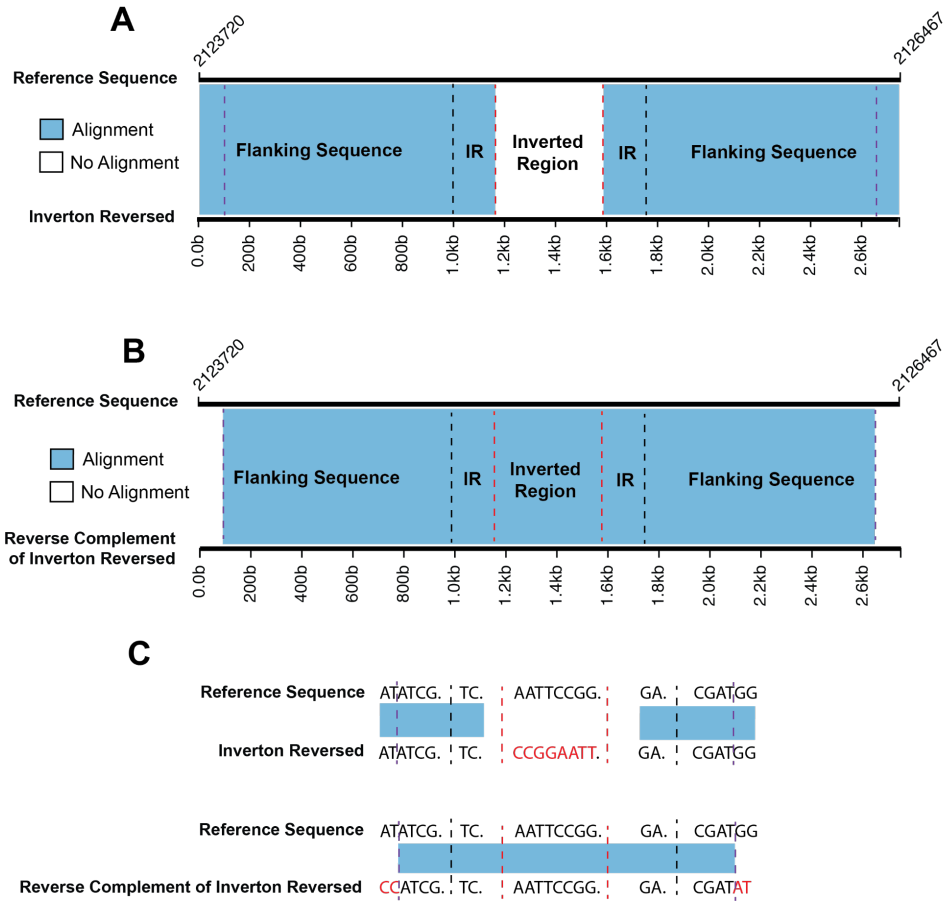

Fig. S3. Very long (>750bp), near perfect, inverted repeats can lead to false positives. (**A**) Alignment of inverton NZ_CP025371.1:2124719-2124870-2125316-2125467, with its invertible sequence inverted, against the *B. pertussis* genome leads to perfect alignment of flanking and IR regions as expected. 'Reference genome' refers to the *B. pertussis* reference genome sequence. 'Inverton reversed' refers to the putative inverton sequence and flanking sequence, with the invertible sequence inverted. Red dashed lines indicate boundaries of the invertible sequence, black dashed lines indicate boundaries of the inverted repeats as detected by einverted, and purple dashed lines indicate the true boundary of inverted repeats. (**B**) Alignment of the reverse complement of the entire inverton NZ_CP025371.1:2124719-2124870-2125316-2125467 with its invertible sequence inverted and flanking sequence, against the *B. pertussis* genome leads to near perfect alignment (6 mismatches) spanning far into the flanking sequence to the true boundary of the inverted repeats, allowing for reads to map regardless of inverton orientation. (**C**) Example with toy nucleotide sequences. Red nucleotides indicate mismatches.

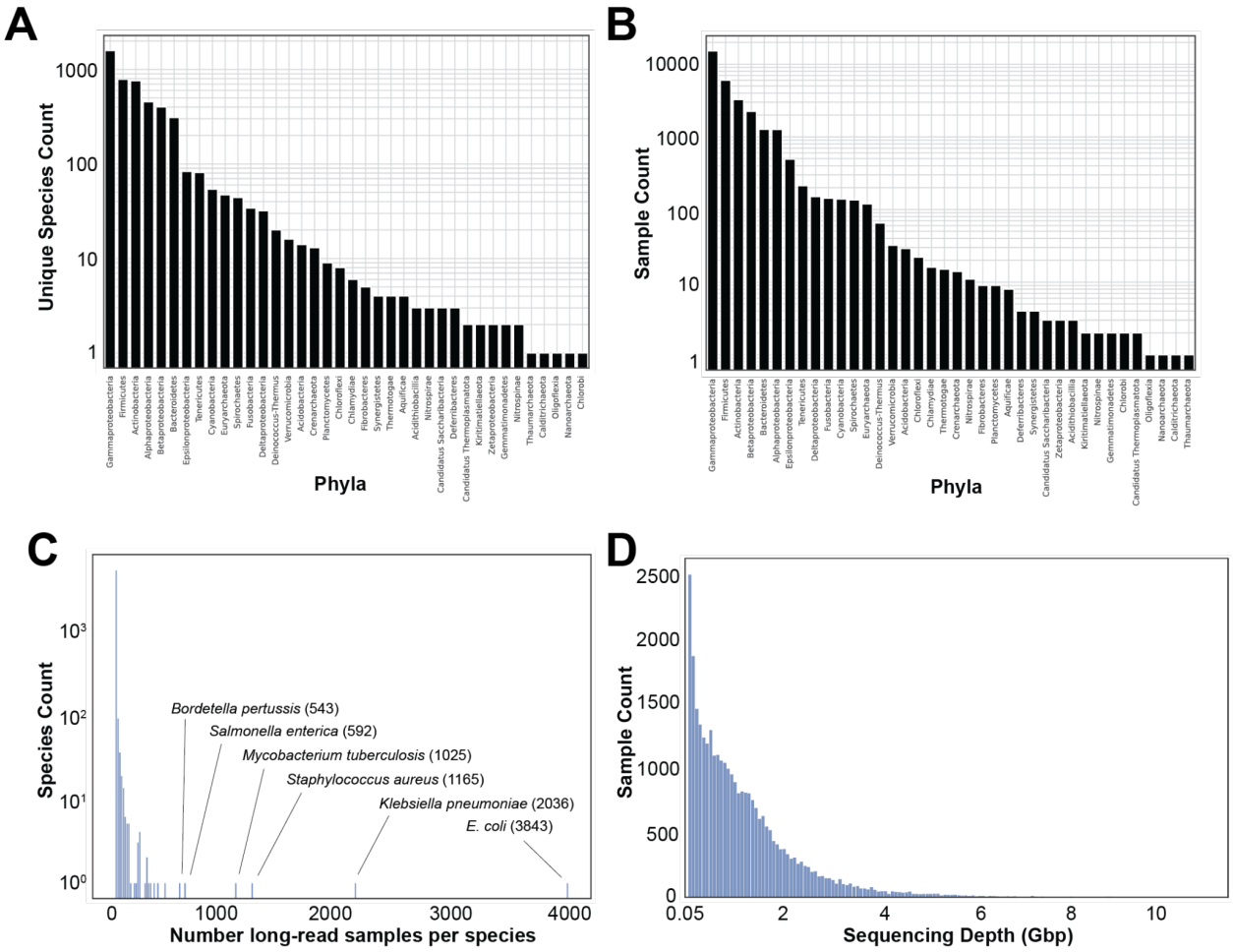

Fig. S4. Overview of SRA long-read isolate sequencing samples analyzed with PhaVa. (**A**) The number of unique species represented in the dataset, grouped by phylum. (**B**) The raw number of sequencing samples, grouped by phylum. (**C**) Histogram of sequencing samples per species. Species with particularly large numbers of samples are labeled. (**D**) A histogram of sequencing depths for all long-read isolate sequencing samples.

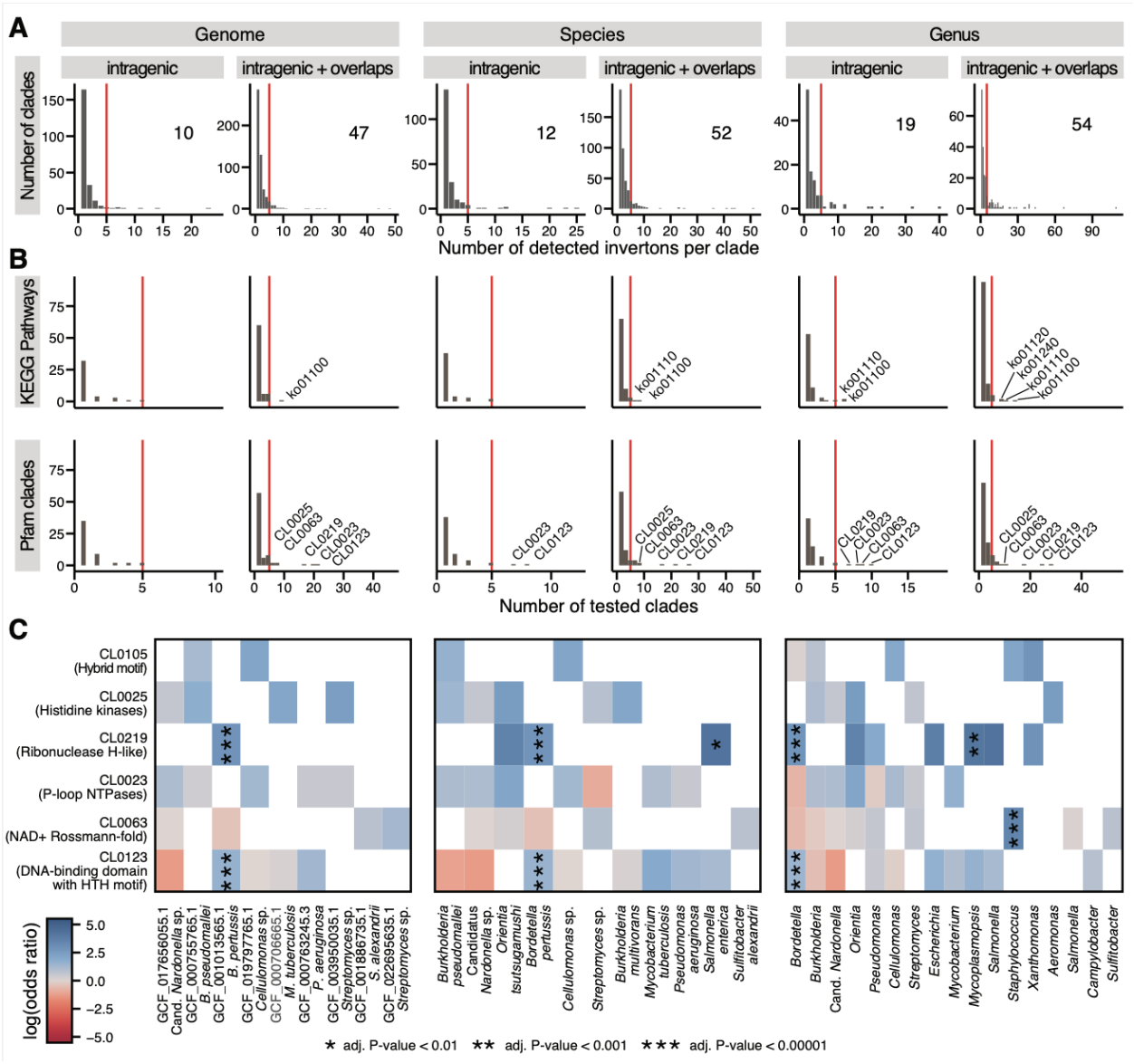

Fig. S5. Intragenic invertons are rare across genomes yet consistently enriched in some Pfam clans. (A) Histograms showing the number of clades (genomes, species, or genera) at various numbers of invertons indicate that invertons are rare, as only one to three invertons can be detected in the majority of clades. Only clades with at least five invertons (red line; number of clades is indicated in the top-right corner of each subplot) were included for the subsequent enrichment analysis. **(B)** KEGG pathways and Pfam clans were tested for enrichment of intragenic (or partial intergenic) invertons in included clades, using a one-sided Fisher's exact test per clade (see Methods). Enrichment was only calculated for sets with at least five invertons associated with genes in the set. Histograms show the number of sets with enrichment score at the number of included clades, showing that most enrichments could be calculated for single

955 clades only. For example, all KEGG pathways associated with enough intragenic invertons for
956 an enrichment analysis on genome-level were specific for each genome. Sets with enrichment
957 scores across at least five clades (red line) are labeled with their corresponding identifiers. **(C)**
958 Heatmap showing the log-odds ratio (effect size for the enrichment of intragenic invertons)
959 across included clades for the six Pfam clans that have enrichment scores on genus-level (see
960 panel B). Stars indicate significance of the enrichment as calculated by Fisher's exact test and
961 corrected for multiple hypothesis testing using the Benjamini-Hochberg procedure.
962

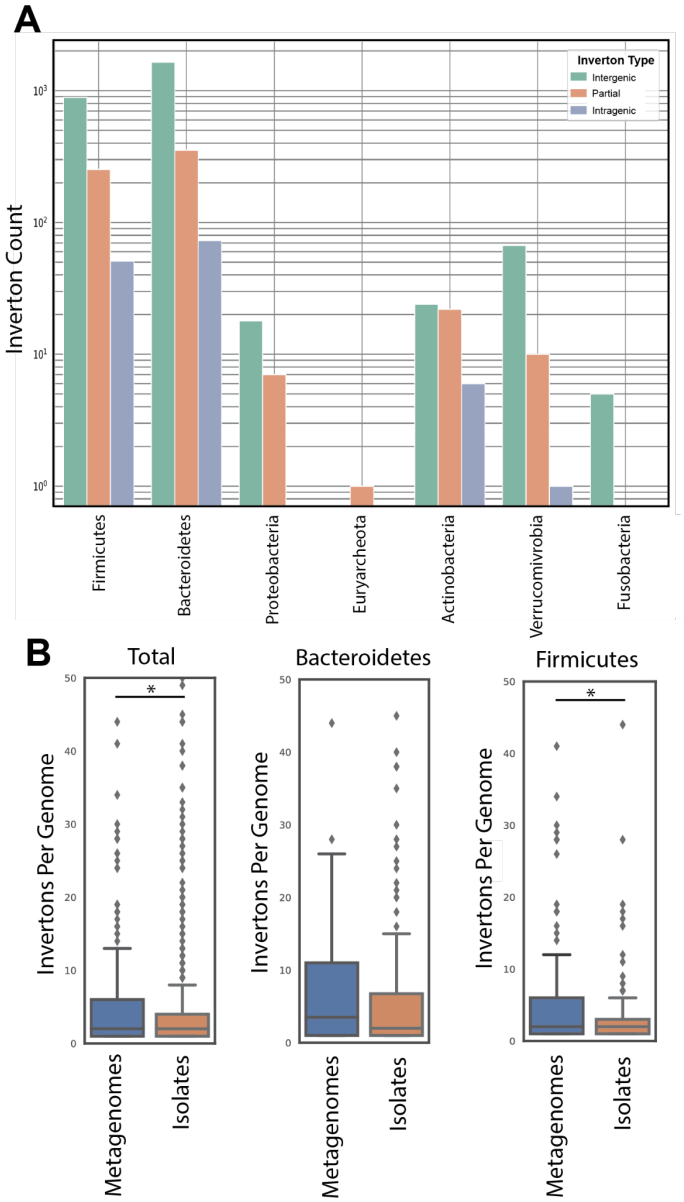

Fig. S6. PhaVa analysis of 210 long-read metagenomes from human stool. (**A**) Counts of invertons identified with PhaVa in 210 stool samples, grouped by phylum and the type of inverton. (**B**) Comparisons of the number of invertons (per genome) found in metagenomic datasets vs. SRA isolate sequencing samples. Total refers to all invertons identified, regardless of taxonomic classification. The distribution of inverton counts per species were found to be significantly different between metagenomes and isolate samples in both the Total and Firmicutes comparisons (p=3.35e-05 and p=0.005 respectively) with a Kolmogorov–Smirnov test. Other individual phyla were not compared due to small species counts with invertons in metagenomic samples.

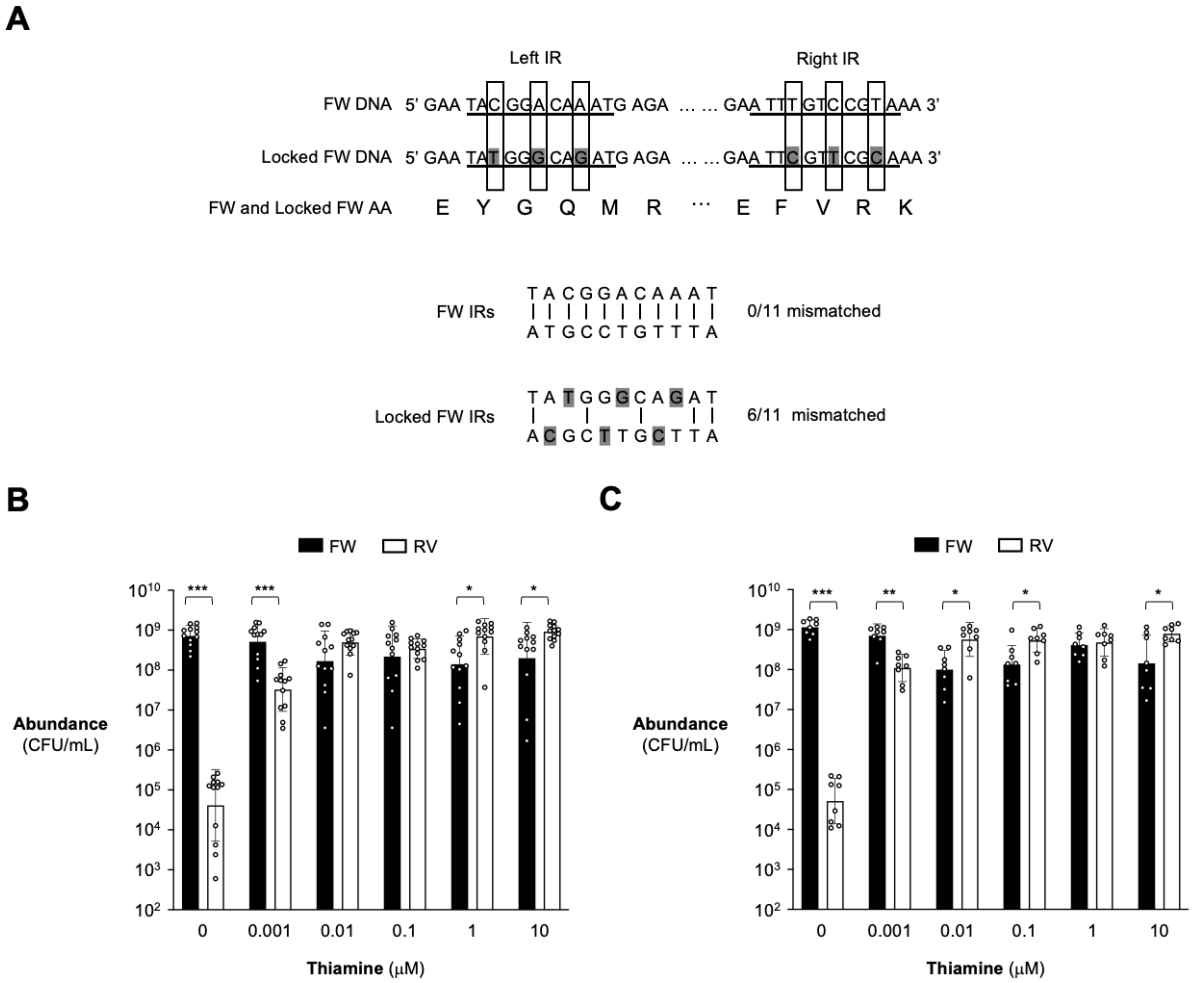

Fig. S7. Locked *thiC* intragenic inverton construction and growth competition. (**A**) Generation of locked intragenic invertons. The forward and locked forward *thiC* IR nucleotide sequences are shown. When possible, the wobble position of each codon corresponding to the IR was mutated to increase mismatches between the two palindromic sequences while maintaining the amino acid sequence. Nucleotides that were mutated are highlighted in gray. (**B-C**) Locked *thiC* strains were competed against each other in thiamine-containing media in a 1:1 ratio. After 40 hours, the abundance of each strain was enumerated using selective agar. Black bars indicate the locked forward strain and white bars indicate the locked reverse strain. Recovered abundances shown here correspond with the competitive index shown in Fig. 4D. In (**B**) the locked forward strain is marked with an erythromycin resistant cassette and the locked reverse strain is marked with a tetracycline resistant cassette. In (**C**) the locked forward strain is marked with a tetracycline resistant cassette and the locked reverse strain is marked with an erythromycin resistant cassette. Geometric mean and geometric standard deviation are shown for replicates conducted across 4-6 independent experiments. For each thiamine concentration a ratio paired t test was performed on the locked forward and locked reverse abundances. ***, $p < 0.001$; **, $p < 0.01$; *, $p < 0.05$.

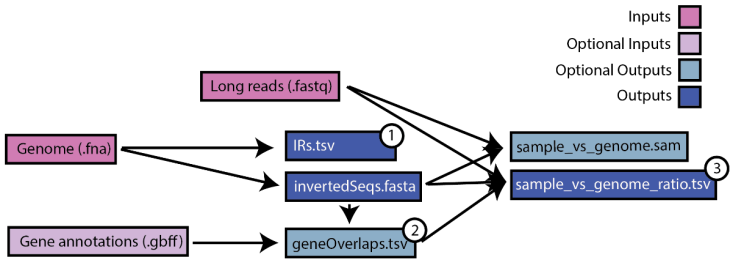

1 IRs.tsv

chromosome	left IR start	left IR stop	right IR start	right IR stop	left IR sequence	invertible sequence	right IR sequence
chr1	1032	1046	1146	1160	ATCG	TACGGATATTACG	CGAT

2 geneOverlaps.tsv

Inverton	gene overlaps	Upstream Gene	Upstream Gene Strand	Upstream Gene Distance	Downstream Gene	Downstream Gene Strand	Downstream Gene Distance
inv1	intragenic BT04	BT03	+	100	BT05	-	150

3 sample_vs_genome_ratio.tsv

Inverton	gene overlaps	forward read #	reverse read #	reverse ratio	sample	Upstream Gene	Upstream Gene Strand	Upstream Gene Distance	Downstream Gene	Downstream Gene Strand	Downstream Gene Distance
inv1	intragenic BT04	15	5	0.25	SRR123	BT03	+	100	BT05	-	150

Figure S8: Inputs and outputs of a variation_wf PhaVa run. Output tables of particular interest are labeled and shown below the diagram with example output.

Strain name	Source	Identifier
Bacteroides thetaiotaomicron VPI-5482 Δ*tdk*	[79]	WT
Bacteroides thetaiotaomicron VPI-5482 Δ*tdk* ΔBT0650	this study	RC131
Bacteroides thetaiotaomicron VPI-5482 Δ*tdk* BT0650 locked RV	this study	RC149
Bacteroides thetaiotaomicron VPI-5482 Δ*tdk* BT0650 locked FW	this study	RC134
Bacteroides thetaiotaomicron VPI-5482 Δ*tdk* BT0650 locked FW *NBU2::NBU2_tet*	this study	RC165
Bacteroides thetaiotaomicron VPI-5482 Δ*tdk* BT0650 locked FW *NBU2::NBU2_erm*	this study	RC 166
Bacteroides thetaiotaomicron VPI-5482 Δ*tdk* BT0650 locked RV *NBU2::NBU2_erm*	this study	RC164
Bacteroides thetaiotaomicron VPI-5482 Δ*tdk* BT0650 locked RV *NBU2::NBU2_tet*	this study	RC163
E. coli S17-1 λ*pir*; *zxx::*RP4 2-(Tetr::Mu) (Kanr::Tn7) λ*pir*	[80]	S17-1 λpir
E. coli DH5α *λpir; F- endA1 hsdR17 (r-m+) supE44 thi-1 recA1 gyrA relA1* Δ*(lacZYA-argF)U189* φ*80lacZ*Δ*M15 λpir*	[81]	DH5α λpir

996
997 **Table S1. Strains used in this study**
998

Recombinant DNA	Identifier	Source
pKNOCK-*bla*-*ermGb*::*tdk*	pExchange	[79]
pExchange BT0650 KO	pRBC20	this study
pExchange BT0650 locked FW	pRBC21	this study
pExchange BT0650 locked RV	pRBC22	this study
pNBU2_tet	tetR	[24]
pNBU2_erm	ermR	[24]

999
1000 **Table S2. Recombinant DNA used in this study**
1001

1002 **Acknowledgments:** We thank Nora Enright, Danica Schmidtke, Aravind Natarajan, Jack Diaz
1003 Shanahan, Dylan Maghini, Mai Dvorak, Alvin Han, Meena Chakraborty, and Bhatt Lab
1004 members for helpful conversations and scientific advice regarding this project. We also thank
1005 Wenhan Zhu for plasmids (pNBU2_tet and pNBU2_erm) and Sebastian Winter for the strain
1006 (DH5α) that were used in the context of this project. We also thank Daniel Haft and Francoise
1007 Thibaud-Nissen at NCBI for helpful discussion about accessing SRA long-read datasets.
1008 **Funding:**
1009 National Institutes of Health R01 AI148623 (ASB)
1010 National Institutes of Health R01 AI143757 (ASB)
1011 Stand Up 2 Cancer Foundation
1012 National Institutes of Health T32 training Grant HG000044 (RBC)
1013 National Institutes of Health T32 training Grant HL120824 (PTW)
1014 **Author Contributions:**
1015 Conceptualization: RBC, PTW, ASB
1016 Methodology: RBC, PTW, JW
1017 Investigation: RBC, PTW, JW, RMP, GZMG, ASH, MOG, EFB, AMM
1018 Visualization: RBC, PTW, JW, RMP
1019 Funding acquisition: ASB
1020 Project administration: RBC, PTW, ASB
1021 Supervision: RBC, PTW, ASB
1022 Writing – original draft: RBC, PTW, ASB
1023 Writing – review & editing: RBC, PTW, JW, RMP, GZMG, ASH, MOG, EFB, AMM,
1024 ASB
1025
1026 **Competing Interests:** Authors declare that they have no competing interests.
1027 **Data and materials availability:** PhaVa is available at (https://github.com/patrickwest/PhaVa).
1028 Short-read adult HCT stool sequencing data was previously published and is available at (NCBI
1029 BioProject ID PRJNA707487). Short-read pediatric HCT stool sequencing data was previously
1030 published and is available at (NCBI BioProject ID PRJNA787952). Long-read metagenomic
1031 sequencing data was previously published and is available at BioProject PRJNA820119 and
1032 BioProject PRJNA940499. Assembled metagenomic contigs will be made available after

publication at https://doi.org/10.5281/zenodo.7662825. A list of accession numbers for long-read isolate sequencing data is available in supplementary file Data S5.

Supplementary Information is available for this paper.

Extended Data Tables

Data S1. *B. theta* intragenic invertons identified from short-read metagenomic sequencing samples.

Data S2. Archaeal invertons identified from long-read isolate sequencing samples.

Data S3. Invertons identified from long-read isolate sequencing samples.

Data S4. Dereplicated invertons identified from long-read metagenomic sequencing samples.

Data S5. List of accession numbers and associated metadata for long-read isolate sequencing samples.

Data S6. Primers used in this study.

Data S7. Simulated read datasets.

Data S8. Additional sequences.

Correspondence and requests for materials should be addressed to Ami Bhatt (asbhatt@stanford.edu).